RESEARCH | Article in Press

Network-targeted neurophysiological biomarkers of dysconnectivity and cognitive decline in Alzheimer's disease

Giacomo Bertazzoli · Elisa Canu · Chiara Bagattini · Fabiola Freri · Natale Salvatore Bonfiglio · Debora Brignani · Martina Bulgari · Veronica Castelnovo · Mara Delai · Elisabetta Ferrari · Claudia Fracassi · Peter J. Fried · Delia Lucarelli · Eleonora Marcantoni · Moira Marizzoni · Annamaria Cattaneo · Valentina Nicolosi · Giulia Quattrini · Silvia Saglia · Michela Pievani · Vincenzo Romei · Antonietta Stango · Massimo Filippi · Federica Agosta · Marta Bortoletto

Received: 9 April 2026 / Accepted: 31 August 2026
© The Author(s) 2026

Abstract

Background Alzheimer's disease (AD) is marked by progressive network disconnection that begins decades before symptoms emerge, yet detecting early functional disruptions remains a key challenge. Transcranial magnetic stimulation combined with electroencephalography (TMS–EEG) provides a direct, non-invasive probe of cortical dynamics and may yield biomarkers that index cortical network dysfunction, track progression, and inform personalized neuromodulation strategies.

Methods We enrolled 86 participants: 28 HC (mean age 69.7 ± 6.0, 15 female), 27 MCI (73.1 ± 5.2, 16 female), and 31 ADD (75.8 ± 4.9, 17 female). TMS–EEG targeted individualized default mode (DMN) and executive control (ECN) network nodes identified via resting-state fMRI. Using a data-driven strategy, we extracted early TMS-evoked potential (TEP) components within 50 ms. We assessed group differences, associations with hippocampal volume, white matter integrity, and cognition, and prediction of cognitive decline over ~1.5 years ($n = 55$).

Results After left DMN stimulation, the contralateral frontal N20F peak was increased in both MCI (P-adj. = 0.0001, $\Delta = 1.89$ μV) and ADD (P-adj. = 0.0003, $\Delta = 1.76$ μV) relative to HC, achieving an AUC of 0.82 for HC-versus-MCI classification. In the ECN, N20C amplitude showed a diagnosis-by-hemisphere interaction: reduced in MCI after left stimulation (P-adj. = 0.036, $\Delta = -13.64$ μV) but increased in MCI and ADD after right stimulation (P-adj. = 0.028, $\Delta = 14.59$ μV and P-adj. = 0.048, $\Delta = 10.30$ μV). Left DMN N20C amplitude correlated with superior longitudinal fasciculus integrity ($P = 0.009$, $\beta = 37.15$). TEPs were selectively linked to executive function: in ADD, larger left ECN N20F predicted worse Trail Making Test scores (P-adj. = 0.003, $\beta = -24.35$).

This Article in Press is shared early to give you faster access to new research. It is citable and carries a permanent DOI. The final edited version will replace it automatically.

Federica Agosta and Marta Bortoletto contributed equally as senior authors.

Longitudinally, lower left DMN N20C predicted steeper global cognitive decline (β = 0.74, $P = 0.014$), and right ECN N20C predicted executive decline in MCI (β = −35.15, $P = 0.0004$).

Conclusions Early network-targeted TEPs capture functional alterations linked to AD progression. Limitations include the moderate sample size, clinical rather than biomarker-confirmed diagnosis, and single-site design. These network-specific, hemisphere-sensitive measures may serve as biomarkers for diagnosis, tracking, and prognosis of cognitive decline, and could inform personalized network-targeted neuromodulation in AD.

Trial registration Not applicable (observational study).

Keywords AD dementia · Mild cognitive impairment · Transcranial magnetic stimulation · EEG · TMS-EEG · TMS-evoked potentials · Brain networks

Background

Dementia is among the most pressing medical challenges facing aging societies, with Alzheimer's disease (AD) as the leading cause [1, 2]. The disease begins decades before symptoms appear, as abnormal proteins, amyloid-beta and hyperphosphorylated tau, accumulate in the brain, disrupting communication between neurons and progressively damaging large-scale brain networks [3, 4].

Brain imaging studies reveal that Alzheimer's pathology tends to spread along specific brain networks [4, 5]. Two networks are particularly vulnerable: the default mode network (DMN) supports high-level cognitive functions such as memory retrieval and mental imagery, showing progressive breakdown that closely tracks Alzheimer's pathology [6, 7]. The executive control network (ECN) governs planning and mental flexibility, and its dysfunction contributes to characteristic cognitive deficits in AD [8, 9]. Studies examining the brain's white matter show deterioration of structural connections as AD progresses, spreading from areas with highest accumulation of pathology throughout the brain [10, 11].

PET and fluid biomarkers allow accurate in vivo detection of amyloid-β and tau, and the recent development of blood-based assays is making the biological diagnosis of AD pathology increasingly accessible [12, 13]. However, these molecular markers index the presence and burden of pathology rather than the state of ongoing cortical function. Amyloid and tau PET carry substantial prognostic value, particularly in combination [12, 14]; nonetheless, considerable inter-individual variability in the timing and rate of cognitive decline remains, and none of these markers directly indexes how the cortex is functioning as the disease evolves. Established structural biomarkers, such as hippocampal volume and cortical thinning, capture downstream tissue-level effects of pathology but emerge relatively late in the disease course [15, 16]. Functional neuroimaging modalities such as resting-state fMRI and FDG-PET provide indirect proxies of neuronal dynamics, as they are inferred from hemodynamic or metabolic signals rather than from direct measurements of cortical activity [17, 18]. To complement pathology biomarkers, there is therefore a pressing need for measures that directly index how the brain is functionally responding to AD pathology, both to support prognosis at the individual level and to monitor neuronal effects of the new wave of disease-modifying treatments.

Neurophysiological techniques directly measure the electrical activity of cortical neurons. Electroencephalography (EEG) records, through scalp electrodes, the field potentials generated by synchronous neuronal activity with millisecond temporal resolution, and resting-state and task-related EEG have revealed slowing of oscillatory rhythms, reduced signal complexity, and altered functional connectivity in AD [19, 20]. However, EEG offers limited insight into the excitability of specific cortical sites. Transcranial magnetic stimulation (TMS) addresses this limitation by delivering brief magnetic pulses through a coil placed over the scalp; these pulses induce an electric field (iEF) in the underlying cortical tissue that depolarizes neurons and triggers a measurable neural response [21–23]. The magnitude of this response depends on the strength of the iEF and on the state of the cortex that can be altered by aging and atrophy [24–29]. When TMS is combined with EEG (TMS–EEG), it is possible to record TMS-evoked potentials (TEPs) [30]. This perturbational approach provides causal, task-independent

access to local cortical excitability and to effective connectivity that cannot be derived from spontaneous EEG [31], and has proven valuable across neurological and psychiatric disorders [32–35]. By probing cortical physiology directly and in vivo, TEPs offer a functional readout of how AD pathology affects neuronal functioning, complementing molecular and structural biomarkers and potentially indexing the brain's neurophysiological response and resilience to the disease [36, 37].

In AD, TMS–EEG studies consistently reveal altered brain responses. Early responses occurring within the first 50 milliseconds after stimulation are often abnormal, with some studies reporting reduced responses [38–42], and others reporting exaggerated responses compared with healthy older adults [43–50]. These early changes have been linked to clinical severity, with larger responses sometimes associated with worse cognition and executive function [39, 43, 46]. Studies have also revealed reduced brain oscillations, decreased signal complexity, and altered responsiveness, all pointing to disrupted excitability and connectivity in networks affected by AD [51–56].

However, methodological limitations may explain inconsistencies across studies. Most TMS–EEG studies in AD have stimulated predefined anatomical locations rather than targeting specific brain networks known to be disrupted. Only one recent study has begun addressing this gap by targeting disrupted networks [50]. Furthermore, most studies have focused on a single hemisphere, typically the left, overlooking possible interhemispheric differences that could be critical for understanding disease mechanisms. Finally, lack of longitudinal follow-up limits understanding of whether these brain responses can predict future cognitive decline.

Because the prognostic value of such measures will ultimately need to be tested in preclinical populations, a necessary first step is to establish whether network-targeted TMS–EEG captures disease-related alterations along the symptomatic phase of AD. In this study, we therefore tested whether network-targeted TMS–EEG [57] i.e., stimulating individualized nodes within the DMN and ECN, can capture alterations in brain excitability across the symptomatic AD spectrum, from MCI to AD dementia. Specifically, we asked whether (1) early brain responses differentiate between healthy older adults, individuals with mild cognitive impairment (MCI), and those with AD dementia (ADD), examining both hemispheres to reveal symmetrical or lateralized dysfunction; (2) these network-based responses relate to established structural changes such as hippocampal atrophy and white matter degeneration; (3) these measures associate with cognitive performance; and (4) predict cognitive decline over approximately 1.5 years of follow-up.

Methods

Participants

A total of 79 patients with clinical diagnosis of MCI ($n = 38$) or ADD ($n = 41$) were prospectively enrolled at the IRCCS S. Giovanni di Dio, Fatebenefratelli of Brescia, Italy between 2016 and 2024. To maximize the inclusion of typical cases of MCI and AD, we selected patients who: received a clinical diagnosis of amnestic MCI or probable AD dementia [58, 59]; had a Mini Mental State Examination (MMSE) score ≥ 24 (for MCI) or ≥ 16 (for ADD); were aged between 60 and 85 years. Patients' diagnoses were supported by at least one of the following AD or neurodegenerative biomarker: cerebrospinal fluid biomarker (CSF) profile suggestive of AD pathology; temporo-parietal hypometabolism evident at the FDG-PET; hippocampal atrophy detected at the MRI.

Detailed biomarker availability for each diagnostic group is reported in Supplementary Methods ("Alzheimer's disease biomarkers assessment"). Thirty-five HC were recruited by word-of-mouth among participants unrelated to the patient population. All controls were recruited based on the following criteria: age between 60 and 85 years, no family history of neurodegenerative diseases, and normal neurological and cognitive assessment (MMSE ≥ 27). Exclusion criteria for all participants were: medical illnesses or substance abuse that could interfere with cognitive functioning; any (other) major systemic, psychiatric, or neurological illnesses; (other) causes of focal or diffuse brain damage, including lacunae and extensive cerebrovascular disorders at a routine MRI; any contraindications for performing TMS and/or MRI. Safety screening for MRI and TMS compatibility [60, 61] was

performed together with screening of ongoing pharmacological therapy. Of the initial sample of 114 participants, 20 participants met the exclusion criteria, and 8 dropped out of the study. The final sample included 58 patients [27 MCI (age 73.1 ± 5.2 SD, 16 female), 31 ADD (age 75.8 ± 4.9 SD, 17 female)] and 28 HC (age 69.7 ± 6.0 SD, 15 female) (Table 1). The final baseline sample underwent the experimental procedure that included a comprehensive neuropsychological assessment, one MRI session, and one TMS–EEG session (see details below). From the final sample, 55 participants [23 HC (age 69.26 ± 6.08 SD, 13 female), 10 MCI (age 72.60 ± 5.50 SD, 7 female) and 22 ADD (age 76.09 ± 5.23 SD, 12 female)] came back for a neuropsychological re-test session ~ 1.5 years later (range 1.21–1.87 years). All procedures were performed according to the Declaration of Helsinki. Local ethical standards committee on human experimentation approved the study protocol (no: 33/2018). Written informed consent was obtained from participants with capacity to consent, or from their legally authorized representatives when capacity was lacking. In these cases, study procedures were also explained to participants in simple terms, and participation proceeded only if they showed no signs of distress or unwillingness. Sample sizes were estimated based on effect sizes from prior TMS–EEG studies in AD. Bagattini et al. [43], using a comparable protocol in our laboratory, reported large effects for TEP amplitude associations with disease severity (R^2 = 0.20, f^2 = 0.25) and fair classification performance between severity subgroups (AUC = 0.78). Other TMS–EEG studies in AD populations have consistently reported medium-to-large group differences [38–40, 42, 44, 45]. A power analysis for a one-way design with three groups, assuming a medium-to-large effect (f = 0.35, partial $\eta^2 \approx$ 0.11), α = 0.05, and 80% power, indicated a minimum of approximately 25 participants per group (G*Power 3.1).

Network-targeted TMS-EEG recording

Participants were seated comfortably in a dimly illuminated room while viewing a fixation cross. Single biphasic (anterior-posterior posterior-anterior, AP-PA) TMS pulses were delivered using a 75 mm butterfly coil model

Table 1 Demographic characteristics of participants at baseline and follow-up, stratified by cognitive status. Healthy controls (HC), mild cognitive impairment (MCI), and Alzheimer's disease dementia (ADD). Measures include the Montreal Cognitive Assessment (MoCA) and the Geriatric Depression Scale (GDS). Values are presented as count (percentage) for categorical variables or mean (standard deviation) for continuous variables. Group differences were tested using chi-square tests for categorical variables and one-way ANOVA or Kruskal-Wallis tests for continuous variables, depending on normality and homogeneity of variance assumptions. Effect sizes are reported as Cramér's V for categorical variables and eta-squared (η^2) for continuous variables (small≈0.01, medium≈0.06, large≈0.14). Where a significant difference was found, post-hoc pairwise comparisons were conducted using Tukey's HSD for normally distributed data with equal variances, or Dunn's test with Bonferroni correction otherwise. § = significant difference HC–MCI; ‡ = significant difference HC–ADD; † = significant difference MCI–ADD

Baseline	label	Total *N* (%)	Missing *N*	levels	HC	MCI	ADD	Total	*p*	Eff. Size
					28 (32.6)	27 (31.4)	31 (36)	86		
	Biological sex	86 (100.0)	0	F	15 (53.6)	16 (59.3)	17 (54.8)	48 (55.8)	0.9053	0.0480
				M	13 (46.4)	11 (40.7)	14 (45.2)	38 (44.2)		
	Baseline age	86 (100.0)	0	Mean (SD)	69.75 (6.05)	73.15 (5.2)	75.77 (4.88)	72.99 (5.88)	0.0002‡	0.1820
	Baseline education	86 (100.0)	0	Mean (SD)	12.61 (5.05)	10.96 (4.35)	7.68 (3.84)	10.31 (4.85)	0.0002‡ †	0.1870
	MOCA	86 (100.0)	0	Mean (SD)	26.64 (1.5)	18.19 (4.22)	12.45 (4.65)	18.87 (6.99)	<0.0001§‡†	0.718
	GDS	80 (93.0)	6	Mean (SD)	5.86 (4.77)	4.4 (2.66)	6.81 (4.33)	5.73 (4.13)	0.1056	0.0580
Follow-up	label	Total N (%)	Missing N	levels	HC	MCI	ADD	Total	p	Eff. Size
					23 (41.8)	10 (18.2)	22 (40.0)	55		
	Biological sex	55 (100.0)	0	F	13 (56.5)	7 (70.0)	12 (54.5)	32 (58.2)	0.6978	0.1140
				M	10 (43.5)	3 (30.0)	10 (45.5)	23 (41.8)		
	Follow-up age	55 (100.0)	0	Mean (SD)	70.74 (6.01)	73.9 (5.28)	77.59 (5.13)	74.05 (6.28)	0.0006‡	0.2480
	MOCA	55 (100.0)	0	Mean (SD)	25.78 (3.33)	19.1 (4.2)	9.59 (5.11)	18.09 (8.51)	<0.0001§‡†	0.757
	GDS	55 (100.0)	0	Mean (SD)	6.17 (5.09)	5.1 (5.13)	5.95 (5.31)	5.89 (5.11)	0.8593	0.0060

C–B60 for frontal areas and a MC–B65–HO for parietal sites (same as the C–B60 but with perpendicular handle) connected to a connected to a MagPro X100 stimulator (MagVenture Inc, Alpharetta GA, USA). The motor hotspots corresponding to the left and right first dorsal interosseous (FDI) muscles were determined using a standard procedure: starting from the hand knob region of the precentral gyrus identified through the neuronavigation system (SofTaxic, E.M.S., Bologna, Italy), the coil was moved in a spiral pattern around this area to locate the site that elicited the most consistent motor-evoked potentials (MEPs) in the contralateral FDI. Resting motor threshold (rMT) was determined bilaterally at the FDI hotspots using the best PEST strategy. This strategy allows for a fast and accurate estimation of rMT using maximum–likelihood threshold–hunting procedure [62–64]. This strategy was chosen over the standard Rossini-Rothwell method [65], as it retains accuracy while reducing procedure time, an important consideration in a fragile population such as ours [66]. Stimulation intensity was set at 110% of the mean bilateral rMT.

Stimulation sites were determined individually for each participant. Resting-state functional MRI was preprocessed in FSL v5.0.9 and submitted to single-subject independent component analysis (ICA) using MELODIC. ICA components were spatially matched to predefined DMN and ECN templates from the Shirer et al. functional atlas [67], and the components showing the highest correlation with each template were retained. The selected components were then transformed back into each participant's native anatomical (MPRAGE) space, and cluster analysis was applied to identify local maxima within the network. Parietal DMN targets were selected as the first local maximum falling within the inferior parietal lobule (IPL), and frontal ECN targets as the first local maximum falling within the dorsolateral prefrontal cortex (DLPFC), with anatomical boundaries defined on each participant's MPRAGE based on established anatomical knowledge. Parietal IPL nodes were chosen because they are among the earliest and most affected regions in the DMN in AD [68–71]; frontal DLPFC nodes were targeted as central hubs of the ECN, closely linked to executive deficits in the disease [72–74]. Final targets were further constrained to non-atrophic cortical gray matter, visually verified on each participant's SPM12 gray-matter segmentation and T1-weighted image, and to regions that did not overlap with the other network of interest. In the rare cases of overlap, target falling in CSF, coil-positioning issues, or excessive participant discomfort, the next local maximum within the same network mask was used. All targets were localized with the SofTaxic neuronavigation system to ensure accuracy across sessions. Further details are provided in Supplementary Methods. The individualized target-selection pipeline is illustrated in Supplementary Fig. 1S, and representative single-subject independent components and the corresponding stimulation targets are shown in Supplementary Fig. 2S.

A sham condition was included by placing the coil over Cz with a 3 cm spacer. The sham condition was acquired primarily for quality-control, confirming the successful suppression of auditory and sensory non-transcranial components (absence of an N100–P200 complex). We chose not to use the sham condition as a direct subtractive or contrastive comparator in the main analyses because sham TEPs remain a debated topic in the field [75, 76]: the spacer-on-Cz approach reproduces some peripheral and auditory components of TMS but does not faithfully mimic the somatosensory and biomechanical signature of true cortical stimulation [77], and any subtractive analysis carries assumptions about the comparability of these peripheral inputs across diagnostic groups that we cannot independently verify. The stimulation order was counterbalanced across participants using a Latin square design. For each site, 80 TMS pulses were delivered with a random interstimulus interval between 1.5 and 3 s. Multiple strategies were employed to minimize sensory and muscle artifacts from TMS, including noise-canceling headphones with white noise, foam padding between coil and scalp, and optimized cable orientation (see Hernandez-Pavon et al. [78]). EEG was recorded continuously using a 67-channel TMS-compatible system (BrainAmp DC, Brain Products GmbH) at 5 kHz sampling rate with 0.01–1000 Hz bandpass filtering. Impedances were maintained below 5 kΩ. Full technical specifications are provided in Supplementary Methods.

TMS-EEG signal preprocessing

Continuous EEG was preprocessed offline using a custom pipeline implemented in EEGLAB. The TMS pulse artifact was removed by cutting and cubically interpolating the signal between − 1 and + 10 ms relative to each

pulse, then the data were high-pass filtered at 0.1 Hz and epoched between − 750 and + 750 ms. To suppress residual large-amplitude artifacts we applied the source-estimate-utilizing noise-discarding algorithm (SOUND) [79], which down-weights channel-specific noise on the basis of a spherical lead-field model. Remaining TMS-evoked muscle artifacts were attenuated with signal-space projection–source-informed reconstruction (SSP-SIR) [80] applied in the 0–50 ms window, with the smallest number of principal components capturing the muscle twitches selected by two independent raters in both time and frequency domains. Independent component analysis (Infomax with Picard optimization) was then used to remove ocular and remaining decay components, again by independent rater agreement. Trials and channels that remained noisy were rejected automatically (joint-probability threshold of 5 SD) and by visual inspection. Data were finally low-pass filtered at 70 Hz, notch-filtered at 48–52 Hz, and re-referenced to the average of TP9 and TP10. Full preprocessing steps are reported in Supplementary Methods.

TMS-EEG Peaks

In this study we focused on early TEP peaks i.e., those before 50ms, in line with previous literature [38–40, 42–45, 49, 54] to capture the early response of the cortex to the TMS pulse and exclude slower sensory activations. Peaks were extracted following the collapsed localizer strategy suggested in Luck et al. [81]. This procedure allows for an unbiased extraction of the intervals and electrodes in which to search for a peak in the TEPs before extracting its amplitude. The collapsed localizer strategy is recommended in those cases in which there are no a priori information on *where* and *when* a peak will be in an evoked-potential and allows to safely avoid double dipping in peak extraction. For each stimulation site, we grand-averaged TEPs across all participants and visually identified, in both the time-series and the topographical representations, the peaks present within the first 50 ms. Each group-level peak then defined the search space for subject-level extraction: a time window around the peak latency (the "when") and a region of interest (ROI) comprising the highest-amplitude electrodes at that latency (the "where") (Fig. 1). Within each of these predefined windows and ROIs, subject-level peak candidates were detected automatically and reviewed by a rater blinded to diagnostic group (G.B.). As a sensitivity analysis addressing potential operator subjectivity, peak extraction was also repeated with a fully automated procedure that omits the operator check step (Supplementary Methods); Full details are reported in Supplementary Methods; the MATLAB code for both methods is publicly available at https://github.com/GiacomoBert/GR2016_scripts/tree/main/peak_extraction_script.

Neuropsychological assessment

All participants underwent a comprehensive neuropsychological assessment administered by experienced neuropsychologists, covering the cognitive domains routinely examined in AD: global cognition and disease severity (MMSE [82], MoCA [83], ADAS-Cog [84, 85]), verbal and visuospatial memory (RAVLT [86] immediate and delayed recall, FCSRT [87], digit and spatial span [88, 89], Rey-Osterrieth Complex Figure delayed recall [90]), visuoconstructional abilities (Rey-Osterrieth Complex Figure copy [90]), language (phonemic and semantic fluency) [91], attention and executive function (digit span backward, TMT A and B [92], attentive matrices [93], Stroop [94]), and abstract reasoning (Raven's Coloured Progressive Matrices) [95]. Depressive symptoms were screened with the Geriatric Depression Scale (GDS) [96]. Test administration and scoring followed standard procedures [97]. The full list of tests, together with descriptive statistics, is reported in Supplementary Table 1S.

For the analyses presented in this work, we focused a priori on the cognitive measures most informative for the networks targeted. Specifically, we hypothesized that DMN-targeted TEPs would relate primarily to episodic memory (RAVLT immediate and delayed recall), consistent with the established role of the DMN in memory retrieval [98, 99], and that ECN-targeted TEPs would relate primarily to executive function (TMT B − A), consistent with the role of frontal DLPFC nodes in set-shifting and cognitive control [100, 101]. We also note that the network–domain mapping is not strictly one-to-one: DMN nodes can be recruited during executive tasks [102,

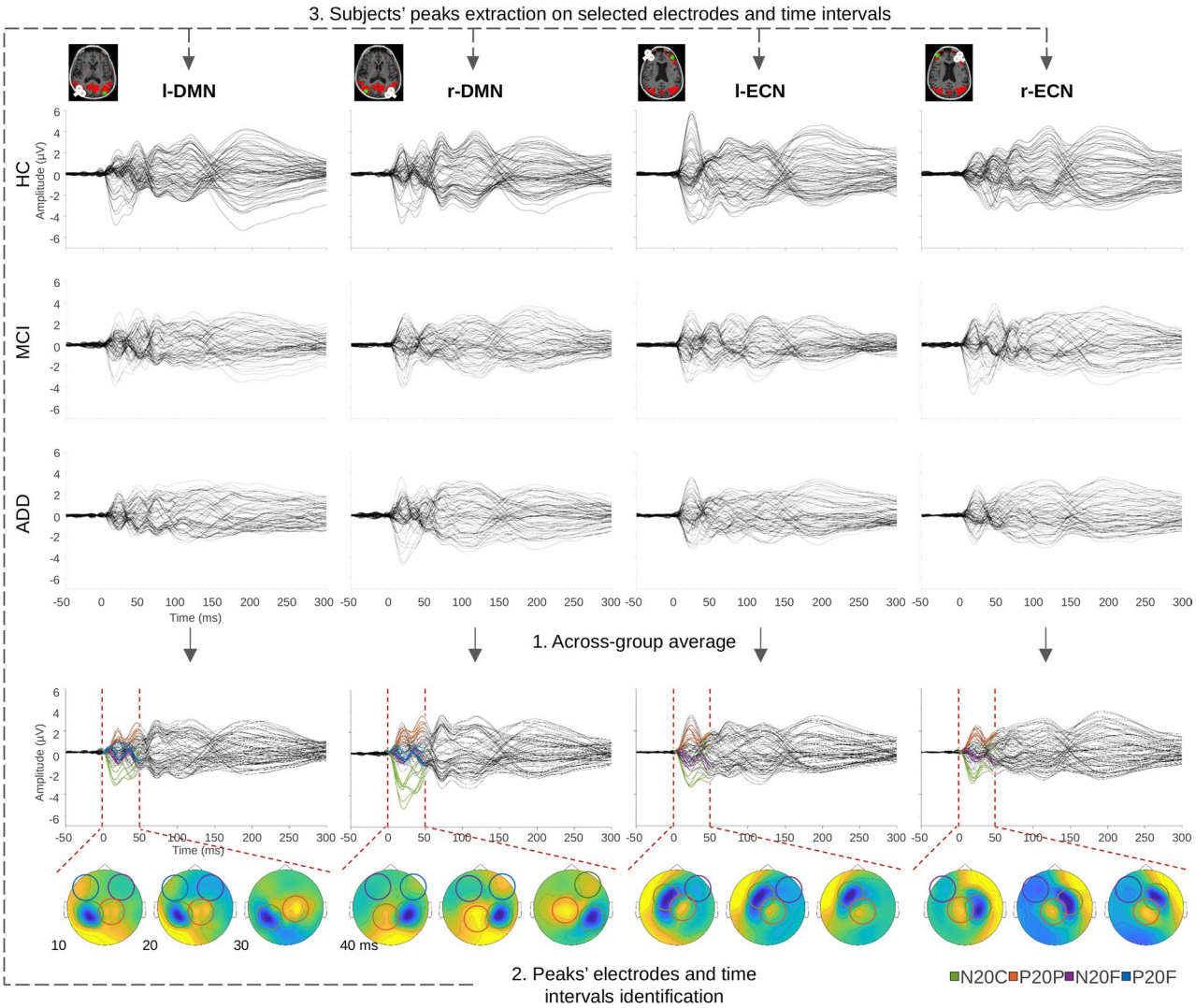

Fig. 1 Collapsed localizer strategy for peaks extraction. Group averages of TMS-evoked potentials (TEPs) recorded from left-right parietal nodes of the default mode network (DMN) and left-right nodes of the executive control network (ECN) in healthy controls (HC), mild-cognitive impairment (MCI) and AD dementia (ADD). The bottom row depicts the grand-grand average across diagnostic groups. The time window of interest (<50ms) is highlighted between vertical dashed lines. Grand-grand average topographical distributions are represented as average between 10–20,20–30 and 30-40ms. Color-coded channels in the grand-grand average butterfly plot and corresponding circles on the topographies highlight the identified TEP peaks N20C, P20P, N20F, and P20F. Y axis depict Amplitude in micro-Volts (μV). X axis depicts time in milliseconds (ms)

103], and compensatory reorganization in AD may further couple DMN responses to executive performance [104, 105]. We therefore tested both networks against both domains. Global cognition (MoCA, ADAS-Cog) was included to capture overall disease severity and longitudinal decline.

MRI measures of hippocampal atrophy and white matter integrity

Structural T1 weighted MRI sequences were processed using FreeSurfer v7.2 to compute individual *hippocampal volumes*, as marker of disease severity [106]. Diffusion weighted imaging (DWI) sequences were acquired to extract indices of *white matter integrity*. We measured white matter integrity in the left and right superior longitudinal fasciculi (SLF), which connect the frontal and parietal stimulation sites, and in the corpus callosum,

focusing on the genu (gCC) and splenium (sCC) that link the left and right DLPFC and IPL, respectively. Fractional anisotropy (*FA*) and mean diffusivity (*MD*) were used in each tract as indices of white matter structural integrity. See Supplementary Methods for details.

Statistical analysis

Statistical analyses were performed in R (www.r-project.org); full model specifications, software details, multiple-comparison handling, and outlier removal are reported in the Supplementary Methods. Group differences in demographics and neuropsychological characteristics across HC, MCI and ADD are reported in Table 1. TMS-EEG peak-extraction metrics (mean amplitude, latency, and number of subjects per peak after outlier removal) are reported in Table 2, and a descriptive inter-peak correlation analysis is reported in the Supplementary Methods and Results.

Network-targeted TEPs peaks' amplitude differences across diagnostic group

To examine whether early network-based TEPs differentiate diagnostic groups, we compared peak amplitudes across HC, MCI, and ADD, separately for each stimulation site within the DMN and ECN. For reference, we ran the same group comparisons for hippocampal volume and white matter integrity. Receiver operating characteristic (ROC) analyses were conducted for TEPs showing significant group effects to assess classification performance. To test whether homologous network nodes in opposite hemispheres provide similar or distinct information, we included hemisphere as a factor in models of TEP amplitudes and examined diagnosis × hemisphere interactions. All linear models in this work, for group comparisons, TEP–structure relationships, TEP–cognition associations, and longitudinal predictions, included age, sex, and education as covariates from the start of model fitting. A bidirectional stepwise procedure was used to retain only terms that contributed to model fit; the predictors of primary interest (diagnosis and, where applicable, its interactions with TEP amplitude and time) were forced to remain in the model. Demographic covariates were always tested, and were dropped only when their unique contribution was non-significant given the other model terms, meaning that the reported diagnosis and TEP effects are not driven by demographic imbalances. iEF and stimulation MNI coordinates were similarly entered as control predictors in the TEP-amplitude models and submitted to the same stepwise procedure. See Supplementary Methods for details.

Relation between network-targeted TEPs, hippocampal volume and white matter integrity

To evaluate whether TEPs reflect structural pathology, we tested correlations between peak amplitudes and MRI-derived measures of hippocampal volume and white matter integrity.

Association between network-targeted TEPs and cognition

To assess whether TEPs are associated to cognition beyond diagnostic status, we modeled associations between peak amplitudes and performance across memory and executive domains, and compared their predictive value to structural measures.

Prognostic power of network-targeted TEPs on longitudinal cognitive changes

To test the prognostic hypothesis, we examined whether baseline TEPs predicted longitudinal changes in cognition over ~1.5 years, again benchmarking their performance against hippocampal and white matter measures.

https://doi.org/10.1186/s13195-026-02176-4

Table 2 Characteristics of TMS-evoked potential (TEP) peaks across study groups following stimulation of Executive Control Network (ECN) and Default Mode Network (DMN) nodes. Data shows early TEP components (< 50ms) recorded during left and right hemispheric stimulation. Peak amplitudes (μV) and latencies (s) are presented as mean (standard deviation) for Healthy Controls (HC), Mild Cognitive Impairment (MCI), and Alzheimer's disease dementia (ADD) groups. Peak nomenclature follows the format: polarity (P=positive, N=negative), approximate latency (20ms), and scalp position (P=parietal, F=frontal, C=coil site). Extraction electrodes indicate the four channels used for peak detection following the collapsed localizer strategy. Missing data points (Missing N) represent unsuccessful peak extractions in individual participants. Relative position indicate position of the peak realtive to stimulation site: rP= Right Parietal; lP= left Parietal; rF= right Frontal; lF= left Frontal; C= controlateral; I= Ipsilateral

label	Total *N*	Missing *N*	extraction electrodes	relative position	HC		MCI		ADD		Total	
					amplitude (μV)	latency (ms)	amplitude (μV)	latency (ms)	amplitude (μV)	latency (ms)	amplitude (μV)	latency (ms)
Total N (%)					28 (32.6)		27 (31.4)		31 (36.0)		86	
P20P - left ECN stim.	86 (100.0)	0	CPz CP2 C2 Pz	rP – C	4.03 (3.28)	22.7 (5.7)	3.83 (2.85)	21.5 (5.8)	3.86 (3.73)	23.1 (4.6)	3.9 (3.29)	22.5 (5.3)
N20F - left ECN stim.	85 (98.8)	1	F2 F6 F4 AF4	rF- C	-4.19 (3.51)	22.7 (5.6)	-3.37 (3.3)	23.6 (5.6)	-4.37 (4.49)	22.2 (6.6)	-4 (3.82)	22.8 (5.9)
N20C - left ECN stim.	86 (100.0)	0	F1 FC1 FC3 C3	lF – I	-8.57 (4.27)	23.9 (5.9)	-6.18 (4.3)	20.3 (4.8)	-5.68 (4.55)	21.9 (5.3)	-6.77 (4.51)	22.1 (5.5)
P20P - right ECN stim.	84 (97.7)	2	CPz CP1 C1 Pz	lP – C	3.5 (3.2)	22.9 (5.9)	3.62 (2.65)	21.8 (4.4)	3.82 (3.45)	22.5 (4.2)	3.65 (3.09)	22.4 (4.9)
N20F - right ECN stim.	84 (97.7)	2	F5 F3 F1 AF3	lF – C	-3.78 (2.99)	22.5 (6.3)	-2.45 (2.29)	22.5 (6.2)	-2 (2.53)	22.3 (5.4)	-2.74 (2.7)	22.4 (5.9)
N20C - right ECN stim.	84 (97.7)	2	CP4 C4 FC4 CP6	rF – I	-5.45 (5.58)	21.5 (7.5)	-6.98 (6.43)	20.7 (5.0)	-6 (5.98)	21.8 (5.2)	-6.13 (5.96)	21.4 (5.9)
P20P - left DMN stim.	86 (100.0)	0	POz CPz CP4 P2	rP – C	3.56 (2.55)	18.5 (3.4)	3.33 (2.12)	20.2 (6.0)	3.85 (2.12)	20.4 (4.9)	3.59 (2.25)	19.7 (4.9)
P20F - left DMN stim.	85 (98.8)	1	F5 F1 F7 FT7	lF – I	2.42 (1.82)	32.5 (4.3)	2.41 (2.32)	34.9 (6.2)	1.9 (2.57)	33.0 (6.2)	2.24 (2.25)	33.4 (5.7)
N20C - left DMN stim.	85 (98.8)	1	P5 CP5 P3 P7	lP – I	-6.74 (6.62)	19.2 (6.2)	-5.69 (6.04)	19.1 (5.9)	-3.62 (5.92)	22.2 (7.4)	-5.31 (6.26)	20.2 (6.6)
N20F - left DMN stim.	82 (95.3)	4	F8 AF4 F4 F6	rF – C	-1.76 (2.99)	20.9 (4.5)	-3.09 (1.52)	19.2 (3.0)	-2.6 (1.82)	19.9 (4.1)	-2.47 (2.24)	20.0 (4.0)
P20P - right DMN stim.	84 (97.7)	2	CP1 P1 CPz P3	lP – C	3.25 (2.32)	19.4 (4.1)	3.62 (2.61)	20.5 (3.0)	4.23 (3.64)	19.8 (3.3)	3.72 (2.94)	19.9 (3.5)
P20F - right DMN stim.	84 (97.7)	2	FCz Fz FC1 F1	lF – C	1.26 (1.45)	35.7 (6.1)	2.07 (1.27)	38.3 (6.2)	2.14 (2.16)	35.9 (6.8)	1.82 (1.72)	36.6 (6.4)
N20C - right DMN stim.	82 (95.3)	4	CP6 P6 TP8 P8	rP – I	-6.72 (6.01)	20.5 (5.9)	-6.55 (5.36)	20.0 (5.5)	-7.69 (5.88)	20.9 (6.2)	-7.02 (5.72)	20.5 (5.8)
N20F - right DMN stim.	81 (94.2)	5	F5 F3 F1 F7	lF – C	-2.21 (1.25)	21.0 (3.6)	-2.25 (1.13)	20.4 (3.2)	-2.17 (2.38)	20.8 (4.2)	-2.21 (1.69)	20.7 (3.7)

Control and post-hoc analyses

(A) Hippocampal volume and white matter integrity differences across diagnostic groups. Hippocampal volume and white matter integrity were compared between diagnostic groups and related to cognition cross-sectionally and longitudinally; AUC values from ROC analyses were computed for HC-vs-MCI, HC-vs-ADD, and MCI-vs-ADD comparisons (see Supplementary Methods for full model specification).
(B) Sensitivity analyses. The robustness of the main findings was assessed through two sensitivity analyses: (i) repeating the principal analyses using TEP amplitudes obtained from a fully automated, operator-independent extraction procedure; and (ii) repeating them on the subset of patients positive for at least one AD-specific molecular biomarker (amyloid PET or CSF), with MCI and ADD analysed both separately and pooled (see Supplementary Methods for full details).
(C) Joint contributions of TEPs and structural biomarkers. To test whether TEPs and structural biomarkers carry overlapping or independent information about cognition and diagnosis, predictor pairs identified as significant in the main analyses were jointly entered into nested regression models: (i) nested linear and linear mixed-effects models for cross-sectional and longitudinal cognitive outcomes, complemented by bidirectional bootstrap mediation analyses; and (ii) multinomial logistic regression for diagnostic classification (see Supplementary Methods for full model specification).
(D) Stimulation intensity and target bias analysis. For each network, we tested whether the induced electric field amplitude and the MNI coordinates of the stimulation site differed across diagnostic groups and could bias TEP amplitude, using linear mixed models with diagnostic group by stimulated hemisphere interactions (see Supplementary Methods for full model specification).
(E) Coil-to-cortex distance sensitivity analysis. To address the possibility that the significant cross-sectional TEP–cognition associations might be driven by atrophy-related differences in stimulation reach rather than by cortical excitability, each focal model was re-fit including the site-matched coil-to-cortex distance (CCD) as an additional covariate. Variance-inflation factors were inspected on a parallel additive version of each model (see Supplementary Methods for full model specification).

Results

Demographics and neuropsychological characteristics

At baseline, 86 participants were included. The ADD group was significantly older than the HC group ($P=0.0001$, $d=1.10$). Education was significantly lower in the ADD group compared to both HC ($P=0.0001$, $d=1.11$) and MCI ($P=0.0084$, $d=0.8$). At follow-up, 55 participants completed the assessment. Demographic details are provided in Table 1. Complete neuropsychological data for all measures are reported in Table 1S. An overview of the neuropsychological evaluation and of the available AD biomarkers in each group are reported in Supplementary Methods, respectively. It is worth noticing that due to the cognitive demands of the TMT-B task, completion rates were particularly low in the ADD group (HC: $n=28/28$, MCI: $n=16/27$, ADD: $n=8/31$). AUC values from ROC analysis for age and education were computed across HC-vs-MCI, HC-vs-ADD, and MCI-vs-ADD comparisons (Supplementary Table 2S; see Supplementary Results, ROC analysis under (A) for full statistics).

Network-targeted TEP peak extraction

The characteristics of peaks are summarized in Table 2; Fig. 1. Following the collapsed localizer strategy, we found four TEPs peaks resulting from DMN stimulation i.e., P20P, P20F, N20C and N20F, and three TEPs resulting from ECN stimulation i.e., P20P, N20C and N20F. The first letter describes the peak's polarity i.e., positive or

negative, in the grand-grand-average. The number following the letter indicates the approximate latency at which these peaks were extracted in the grand-grand-average. The last letter represents the approximate spatial position of the peak on the scalp i.e., parietal, frontal or coil (under the coil). For DMN stimulation, P20P appeared at 19.7±4.9 ms in parietal electrodes contralateral to stimulation with an amplitude of 3.59±2.25 µV; P20F occurred later at 33.4±5.7 ms in ipsilateral frontal electrodes with an amplitude of 2.24±2.25 µV; N20C emerged at 20.2±6.6 ms in ipsilateral parietal electrodes with an amplitude of -5.31±6.26 µV; and N20F appeared at 20.0±4.0 ms in contralateral frontal electrodes with an amplitude of -2.47±2.24 µV. For ECN stimulation, P20P occurred at 22.5±5.3 ms in contralateral parietal electrodes with an amplitude of 3.90±3.29 µV; N20C appeared at 22.1±5.5 ms in ipsilateral frontal electrodes with an amplitude of -6.77±4.51 µV; and N20F emerged at 22.8±5.9 ms in contralateral frontal electrodes with an amplitude of -4.00±3.82 µV. Simple correlations between peaks are reported in Supplementary Results, "Correlation between peaks". A visualization of the grand-average sham condition (Cz stimulation through a 3 cm spacer) is shown in Fig. 3S.

Network-targeted TEPs peaks' amplitude differences across diagnostic group

TEPs peak's amplitude – DMN stimulation

The N20C peak model's ANOVA showed a significant interaction between diagnosis and hemisphere after correction (P adjusted=0.036, η^2p=0.112; sex was removed by stepwise selection, age and education retained). Post-hoc analyses revealed that within the ADD group, there was a significant difference between the left and right hemisphere stimulation (P adjusted=0.002, est. Δ=4.63 µV) such as N20C amplitude was higher after right hemisphere stimulation compared to the left. The model involving the N20F peak revealed significant effects for the interaction between diagnosis and hemisphere of stimulation (P adjusted=0.007, η^2p=0.153; age, sex and education were removed by stepwise selection). Post-hoc analyses showed that when stimulating the left parietal node of the DMN, the amplitude of the N20F peak was significantly higher in both MCI (P adjusted=0.00010, est. Δ=1.89 µV) and ADD groups (P adjusted=0.00027, est. Δ=1.76 µV) compared to HC The remaining DMN peaks (P20P and P20F) did not show significant diagnosis-related effects or interactions after Bonferroni correction (Fig. 2, Supplementary Table 3 S; full results in Supplementary Results (1) DMN). These results indicate altered DMN responses with hemispheric asymmetry and frontal hyperreactivity in patient groups.

ROC analysis

The N20F component after left DMN stimulation achieved an AUC of 0.819 for HC-MCI differentiation with sensitivity of 0.739 and specificity of 0.957 at a critical threshold of -2.29 µV. For HC-ADD discrimination, the N20F component yielded an AUC of 0.752 with sensitivity of 0.652 and specificity of 0.783 at a critical threshold of -1.99 µV (Supplementary Tables 3 S and 2 S; full results in Supplementary Results (1) DMN, ROC analysis).

TEPs peak's amplitude – ECN stimulation

The N20C peak showed a significant interaction between diagnosis and hemisphere (P adjusted=0.011, η^2p=0.078; age, sex and education were removed by stepwise selection). Post-hoc analyses revealed that when stimulating the left hemisphere, MCI showed significantly lower amplitudes compared to HC (P adjusted=0.036, est. Δ = -13.64 µV). The opposite was found in the right hemisphere, where both MCI and ADD groups showed significantly higher amplitudes compared to HC (P adjusted=0.028, est. Δ=14.59 µV and P adjusted=0.048, est. Δ=10.30 µV, respectively). The remaining ECN peaks (P20P and N20F) did not show significant diagnosis-related effects or interactions after Bonferroni correction (Fig. 2, Supplementary Table 4S; full results in

https://doi.org/10.1186/s13195-026-02176-4

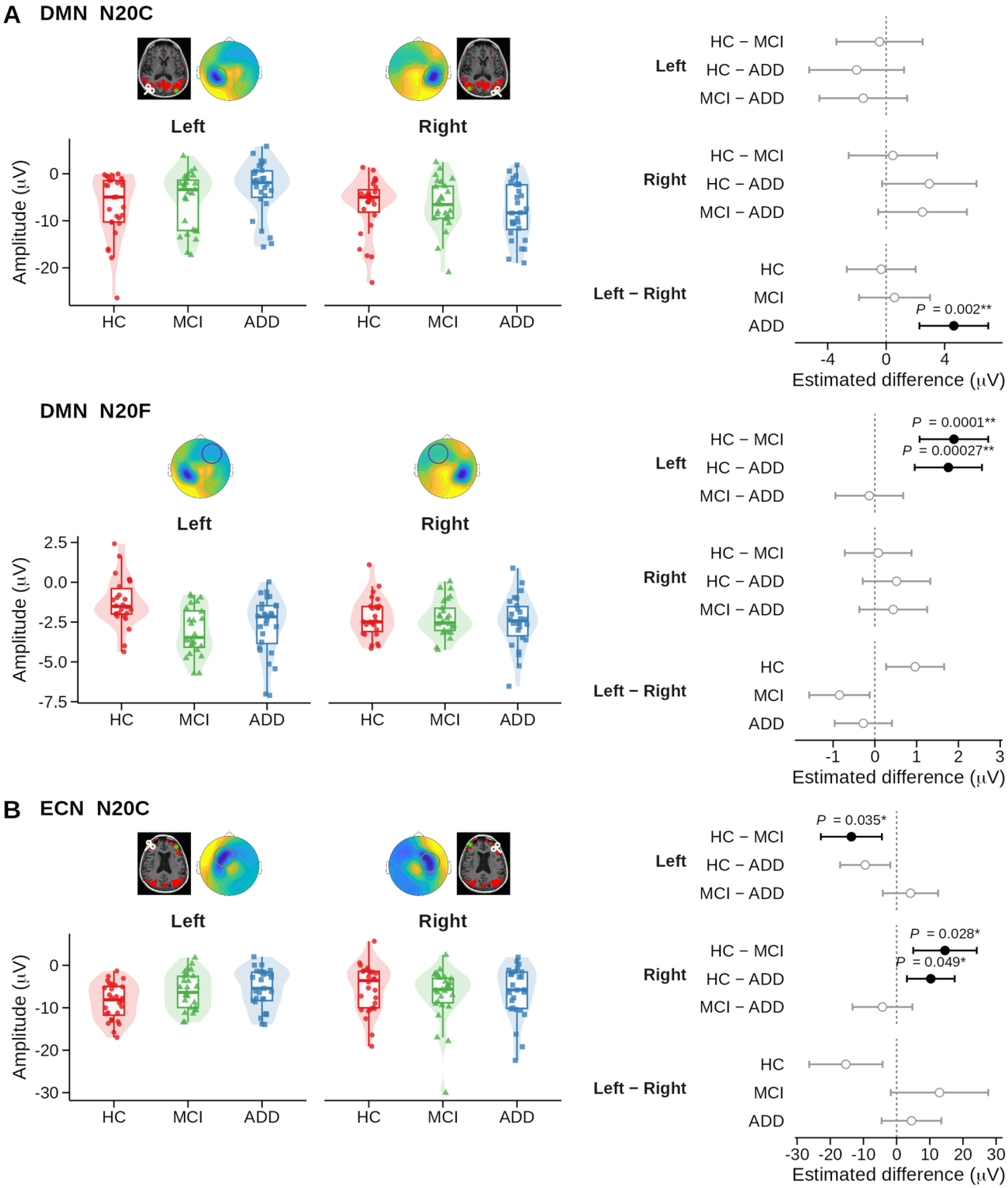

Supplementary Results (1) ECN). These results indicate ECN responses are altered in a hemisphere-dependent manner, with reduced left and increased right frontal activity in patient groups.

Fig. 2 Diagnostic group's difference in peaks' amplitudes. **A** N20C and N20F peaks after DMN stimulation. **B** N20C peak after ECN stimulation. MRI figures represent the estimated site of stimulation. The topography with relative circle represent the average location of the peak. The violin plot represent raw amplitude data in micro-Volts (μV), Y axis. X axis represent diagnostic groups: healthy controls (HC), mild-cognitive impairment (MCI) and Alzheimer's dementia (ADD). Left and Right facets represent hemisphere of stimulation. The bar plots on the right represent the difference in estimated marginal means extracted by the linear mixed models with confidence intervals. Significant differences after p-value correction are labelled with the ANOVA p-value. In the models underlying these effects, sex was removed by stepwise selection for the DMN N20C peak (age and education retained), whereas age, sex and education were all removed for the DMN N20F and ECN N20C peaks

ROC analysis

The N20C component after left ECN stimulation achieved an AUC of 0.648 for HC-MCI differentiation with sensitivity of 0.630 and specificity of 0.607 at a critical threshold of -7.31 μV. After right ECN stimulation, the N20C achieved an AUC of 0.577 for HC-MCI differentiation with sensitivity of 0.926 and specificity of 0.357 at a critical threshold of -1.74 μV. For HC-ADD discrimination, the N20C component after right ECN stimulation yielded an AUC of 0.529 with sensitivity of 0.815 and specificity of 0.286 at a critical threshold of -1.44 μV (Supplementary Fig. 4S, Supplementary Tables 4S and 2 S; full results in Supplementary Results (1) ECN, ROC analysis).

Relation between network-targeted TEPs, hippocampal volume and white matter integrity

DMN TEPs peak's amplitude vs. hippocampal volume and white matter integrity

The N20C peak showed a significant hemisphere-specific relationship with SLF MD (hemisphere × MD interaction: P adjusted = 0.046, β = -38.70 μV; education was removed by stepwise selection, age and sex retained), with significant positive relationship in the left hemisphere (P adjusted = 0.009, β = 37.15 μV) across all diagnostic groups, such as the higher SLF MD i.e., more white matter damage, the smaller the N20C amplitude. No other significant associations between DMN TEP peaks (P20P, P20F, N20C, N20F) and structural markers (hippocampal volume; gCC, sCC, SLF FA/MD) were found after Bonferroni correction (Fig. 3, Supplementary Table 5 S; full results in Supplementary Results (2) DMN).

ECN TEPs peak's amplitude vs. hippocampal volume and white matter integrity

For the three ECN peaks (P20P, N20C, N20F), no significant association with hippocampal volume or white matter integrity (gCC, sCC, SLF FA/MD) was found across either hemisphere after Bonferroni correction (Supplementary Table 6 S; full results in Supplementary Results (2) ECN).

Association between network-targeted TEPs and cognition

TEPs – DMN association with cognition

For each cognitive outcome, separate linear regression models were fit for each DMN peak (P20P, P20F, N20C, N20F) at each stimulation hemisphere (left, right), with peak amplitude in interaction with diagnostic group and age, sex and education as covariates, retained via bidirectional stepwise selection with diagnosis terms kept (see Methods, subsection (3) and Supplementary Methods). For global cognitive function (MoCA, ADAS-cog) and

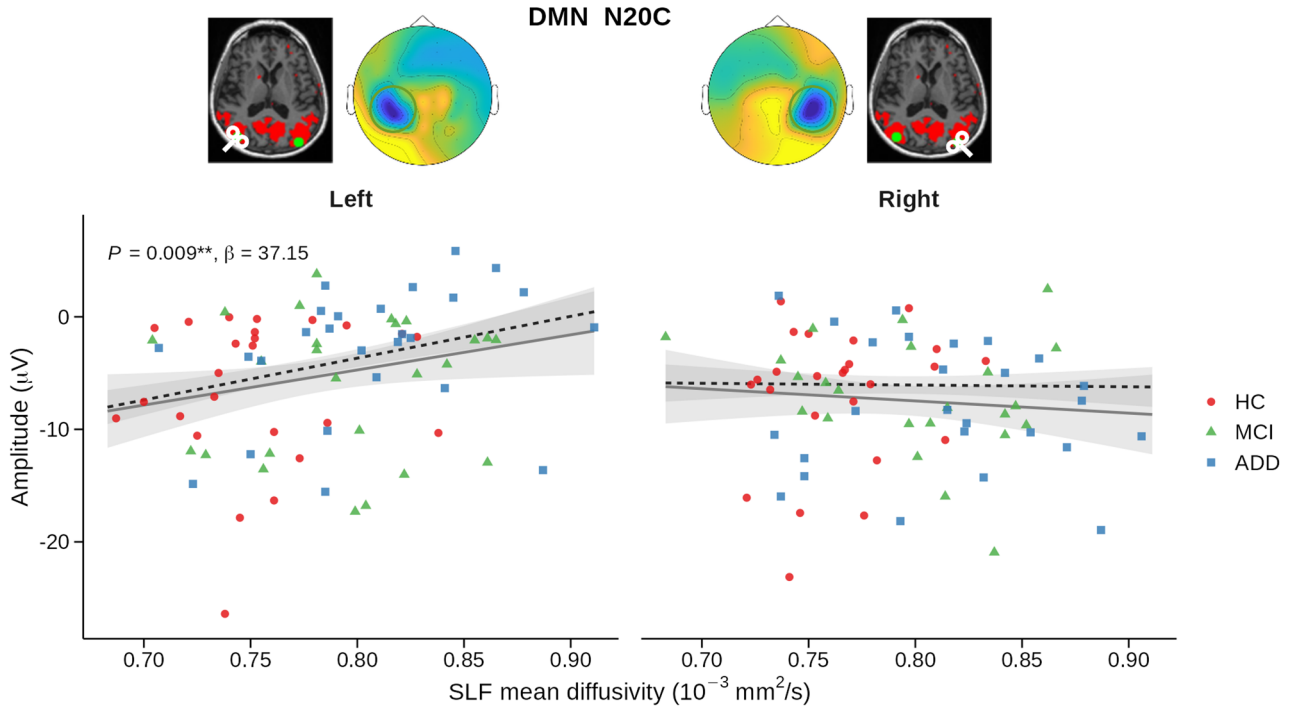

Fig. 3 Default mode network (DMN) N20C relationship with superior longitudinal fasciculi (SLF) mean diffusivity (MD). MRI figures represent the estimated site of stimulation. The topography with relative circle represent the average location of the peak. In each scatterplot Y axis represent raw amplitude data in micro-Volts (μV). X axis represents MD for white matter tracts. Diagnostic groups are color coded: healthy controls (HC) in red, mild-cognitive impairment (MCI) in green and Alzheimer's disease dementia (ADD) in blue. The solid trend line represent raw data trend with standard error. The dashed trend line represent the trend predicted by the model with standard error. In the underlying model, education was removed by stepwise selection (age and sex retained)

memory (RAVLT immediate, RAVLT delayed recall), no peak × diagnosis interaction reached significance for any DMN peak after correction (all P adj > 0.10); in most non-significant models the stepwise procedure eliminated the peak term entirely, indicating that DMN TEP amplitudes did not contribute to predicting these outcomes beyond demographic and diagnostic factors. For executive function (TMT B-A), only P20P amplitude after left hemisphere stimulation showed a significant interaction with diagnostic group: in ADD patients, larger P20P amplitudes were associated with worse executive performance (post-hoc slope β = 27.63 score, P adj = 0.0009; age and sex were removed by stepwise selection, education retained), with non-significant slopes in HC (β = 2.64, P adj = 1.0) and MCI (β = 1.61, P adj = 1.0); all other peak × diagnosis interactions for TMT B-A were non-significant (Fig. 4, Supplementary Table 7 S; full results in Supplementary Results (3) DMN).

TEPs – ECN association with cognition

For global cognitive function (MoCA and ADAS-cog) and memory (RAVLT Immediate and Delayed Recall), no significant effects were found. For executive function (TMT B-A), after left hemisphere stimulation, N20F showed a significant interaction with diagnostic group in ADD patients (P adjusted < 0.0001, β = −24.35 score; age was removed by stepwise selection, sex and education retained), with smaller amplitudes associated with better performance. After right hemisphere stimulation the opposite was found: N20F showed a significant interaction in ADD patients (P adjusted = 0.0009, β = 76.66 score; age, sex and education were removed by stepwise selection) such as more negative amplitudes were associated with better performance The other ECN peaks (P20P, N20C) did not show significant peak × diagnosis interactions on TMT B-A or on any other cognitive

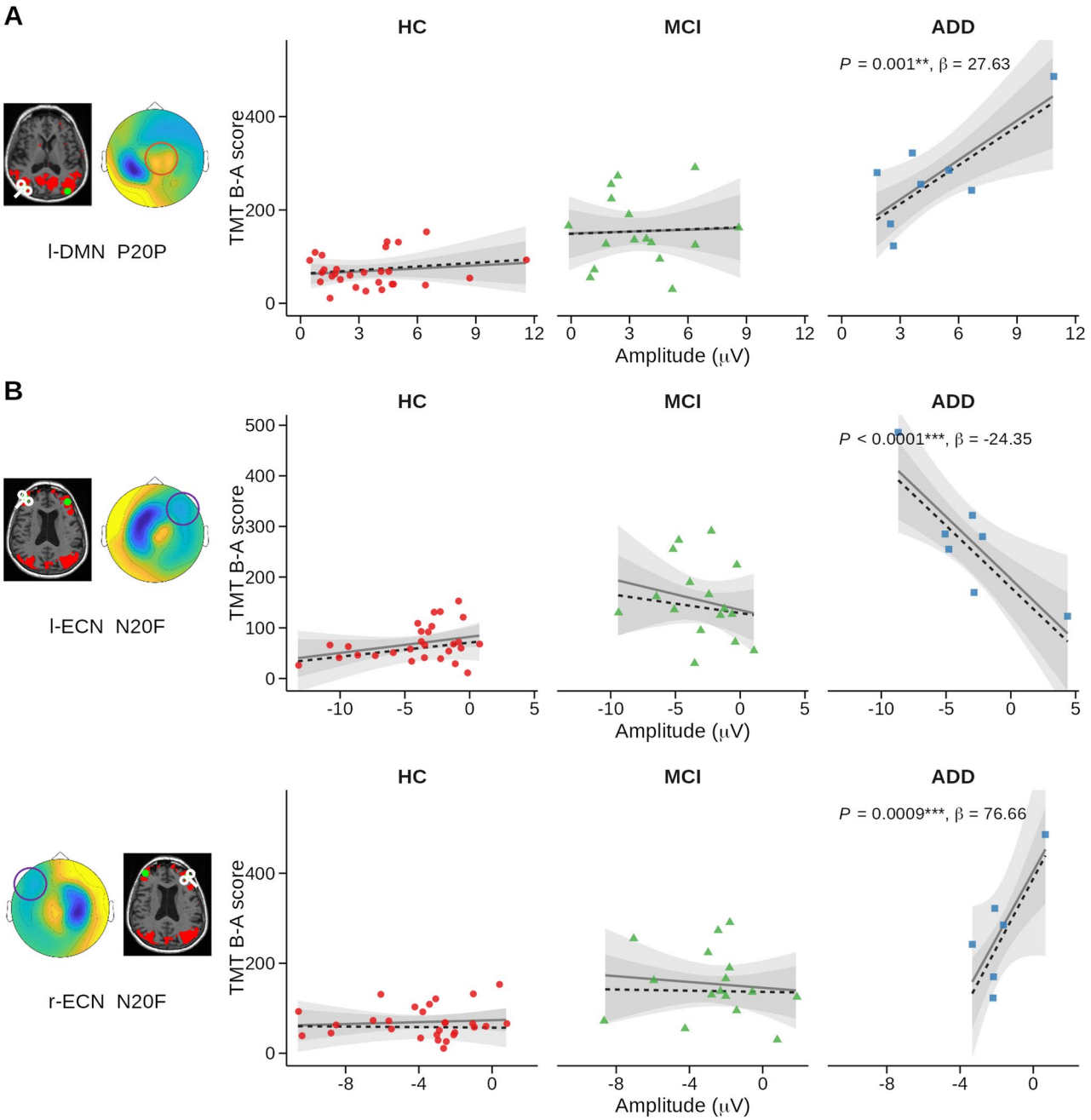

Fig. 4 Cross-sectional relationship between TEPs and cognition. Left Default mode network (DMN) stimulation P20P and left-right executive control network (ECN) stimulation N20F relationship cognitive test TMT B-A. MRI figures represent the estimated site of stimulation. The topography with relative circle represents the average location of the peak. In each scatterplot X axis represent raw amplitude data in micro-Volts (μV). Y axes represent the cognitive test scores. Diagnostic groups are faceted and color coded: healthy controls (HC) in red, mild-cognitive impairment (MCI) in green and AD dementia (ADD) in blue. The solid trend line represents raw data trend with standard error. The dashed trend line represents the trend predicted by the model with standard error. In the underlying models, the DMN P20P peak had age and sex removed by stepwise selection (education retained), the left-ECN N20F peak had age removed (sex and education retained), and the right-ECN N20F peak had age, sex and education all removed

outcome (MoCA, ADAS-cog, RAVLT immediate, RAVLT delayed) after Bonferroni correction (Fig. 4, Supplementary Table 8 S; full results in Supplementary Results (3) ECN).

Prognostic power of network-targeted TEPs on longitudinal cognitive changes

TEPs – DMN predicting cognition's change in time

For MoCA, N20C amplitude from the left hemisphere showed a significant interaction with time (β = 0.74, P adjusted = 0.014; age, sex and education were removed by stepwise selection). The Johnson-Neyman analysis revealed that the effect of time on MoCA was significant when N20C amplitude was outside the interval −0.70 to 1.70 µV, i.e., stronger decline was observed at lower amplitudes (slope at mean–1SD = −0.88, P adjusted = 0.048) compared to higher amplitudes. This suggests that the relation between time and cognitive decline varied depending on the level of N20C amplitude, with lower amplitudes indicating greater vulnerability to decline. No significant interactions between TEP peaks and time were found for memory (RAVLT Immediate and Delayed Recall) or executive function (TMT B–A) after correction The other DMN peaks (P20P, P20F, N20F) showed no significant peak × time or peak × time × diagnosis interactions on any cognitive outcome after Bonferroni correction (Fig. 5, Supplementary Table 9 S; full results in Supplementary Results (4) DMN).

TEPs – ECN predicting cognition's change in time

For ADAS-cog, a significant triple interaction was found between time, diagnosis, and right P20P amplitude (β = −6.05, P adjusted = 0.039; age, sex and education were removed by stepwise selection). In HC, no significant time effects were found. In MCI patients, the relation between time and ADAS-cog scores was significant when P20P amplitudes were outside the interval 0.21 to 1.80 µV, with stronger disease severity at lower amplitudes (slope at mean–1SD = 9.60, P adjusted = 0.0045; slope at mean = 3.68, P adjusted = 0.041). In ADD patients, this relation was significant for P20P amplitudes within the interval −9.43 to 1.53 µV, with consistent decline across amplitude levels (slope at mean–1SD = 6.60, P adjusted < 0.0001; slope at mean = 5.31, P adjusted < 0.0001; slope at mean+1SD = 4.02, P adjusted = 0.026). This indicates that the association between time and disease severity depended on P20P amplitude, with distinct threshold effects across diagnostic groups. No significant interactions with TEP peaks were found for memory (RAVLT Immediate and Delayed Recall). For executive function (TMT B–A), analyses revealed a significant triple interaction between time, diagnosis, and right N20C amplitude (β = −35.15, P adjusted = 0.0004; age, sex and education were removed by stepwise selection). In HC, no significant time effects were found. In MCI patients, the relations between time and performance was significant for N20C amplitudes outside the interval −0.55 to 0.28 µV, showing opposite effects at low versus high amplitudes (slope at mean–1SD = 27.29, P adjusted = 0.015; slope at +1SD = −36.48, P adjusted = 0.0054), reflecting that the direction of change over time depended on N20C amplitude No further significant peak × time or peak × time × diagnosis interactions on memory (RAVLT immediate, RAVLT delayed) or MoCA were observed for the remaining ECN peaks after Bonferroni correction (Fig. 5, Supplementary Table 10 S; full results in Supplementary Results (4) ECN).

Control and post-hoc analyses

(A) Hippocampal volume and white matter integrity differences across diagnostic groups. Hippocampal volume and most white matter integrity measures (splenium MD, bilateral SLF MD, gCC MD) differed significantly across diagnostic groups, were significantly associated with cognitive performance both cross-sectionally and longitudinally, and yielded high diagnostic AUCs (e.g., left hippocampal ratio AUC = 0.92 and splenium

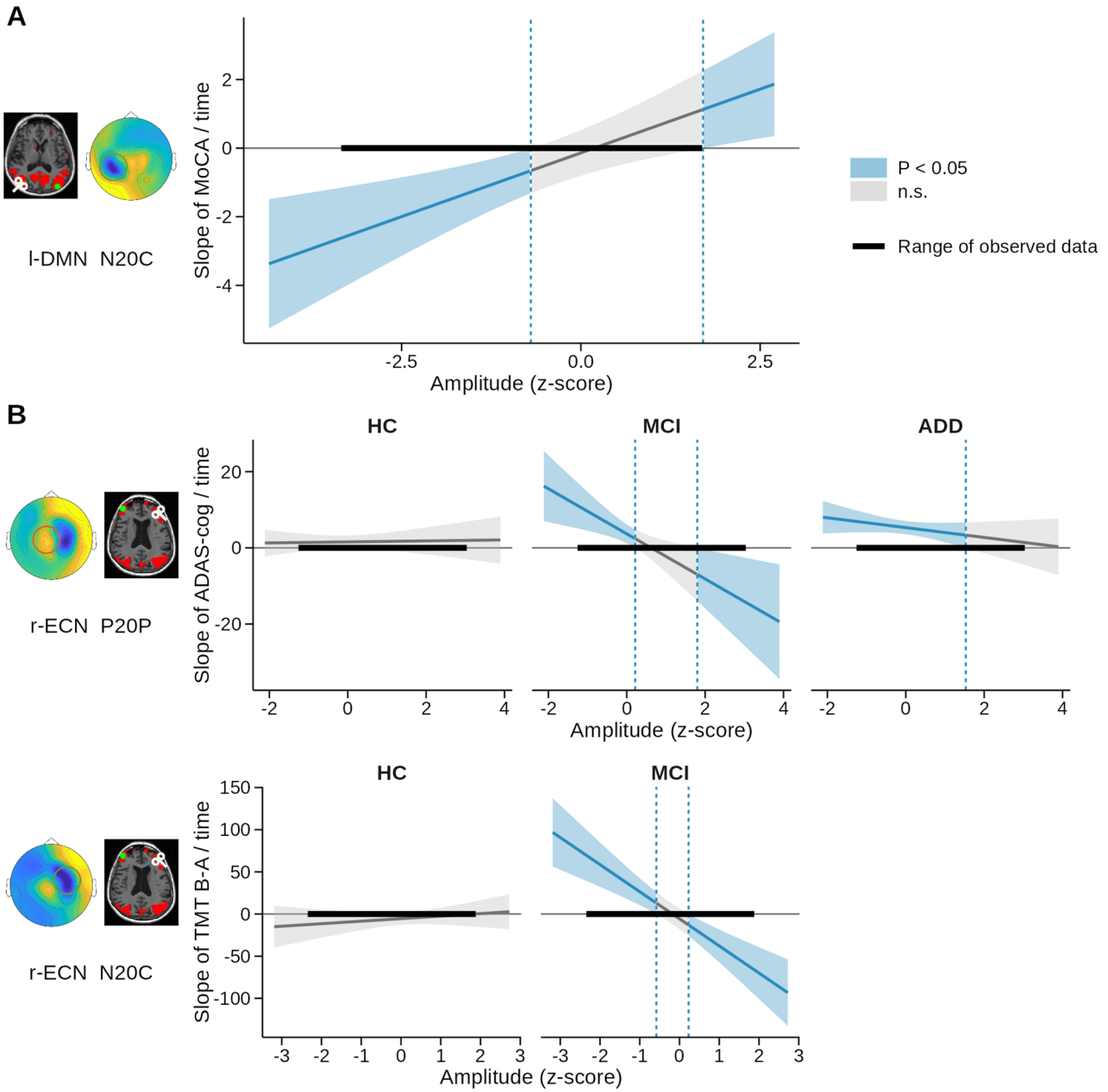

Fig. 5 Longitudinal relationship between TEPs and cognition (**A**) Johnson-Neymann analysis of the left-N20C Default Mode Network (DMN), (**B**) right P20P Executive Control Network (ECN) right N20C ECN for the longitudinal prediction of changes in Montreal Cognitive Assessment (MoCA), Trail Making Test (TMT B-A), and Alzheimer's Disease Assessment Scale-Cognitive Subscale (ADAS-cog). MRI figures represent the estimated site of stimulation. The topography with relative circle represent the average location of the peak. In each plot X axis represent z-scored amplitude data. Y axis represent the slope of the change of cognitive scores in time. Blue areas of the predicted trend represent significant portion of the trend that are significantly different from zero. Black solid zero line represent the range of raw data. When an interaction effect was significant in the model, the plot was faceted for diagnostic group. Healthy controls (HC), mild-cognitive impairment (MCI) and Alzheimer's disease dementia (ADD). In all three underlying longitudinal models (DMN N20C–MoCA, ECN P20P–ADAS-cog and ECN N20C–TMT B-A), age, sex and education were removed by stepwise selection

MD AUC = 0.91 for HC-vs-ADD) (Supplementary Tables 11–13 S, 2 S; full results in Supplementary Results (A)).

(B) Sensitivity analyses. Both sensitivity analyses confirmed the main findings: the principal diagnosis effects on DMN N20F and ECN N20C amplitudes and the prognostic association of left DMN N20C with MoCA decline were retained both when peaks were extracted with the fully automated, operator-independent procedure and when the analyses were restricted to biomarker-positive patients (with MCI and ADD analysed separately and pooled). A few findings (DMN N20C diagnosis × hemisphere interaction; DMN N20C–SLF MD relationship; some cross-sectional TEP–TMT B-A associations) were not retained, consistent with the reduced sample size of the biomarker-positive subset (Supplementary Tables 14–36 S; full results in Supplementary Results (B)).

(C) Joint contributions of TEPs and structural biomarkers. When TEPs and structural biomarkers were entered together as predictors of diagnostic group, left DMN N20F contributed unique variance beyond bilateral hippocampal volume and corpus callosum mean diffusivity (incremental McFadden pseudo-R^2 = 0.13, 0.12 and 0.08 for the right-hippocampal, left-hippocampal and genu corpus callosum pairings, respectively; BH-adjusted $p < 0.01$ in all three); the other diagnosis-related TEPs did not show a similar incremental contribution (remaining $\Delta R^2 \leq 0.023$, none significant after BH correction). For longitudinal cognitive change, three matched TEP × structure × outcome triplets (MoCA, ADAS-cog, TMT B-A) showed largely independent contributions, with each TEP adding only modest variance beyond its structural marker (marginal ΔR^2 = 0.005–0.022) and no significant mediation in either direction (Supplementary Tables 37–39 S; full results in Supplementary Results (C)).

(D) Stimulation intensity and target bias analysis. The induced electric field amplitude was significantly lower in ADD than HC after DMN stimulation ($P = 0.01$), but iEF did not interact with diagnostic group in any TEP-amplitude model, and the MNI coordinates of the stimulation site did not differ across diagnostic groups for either network. Together with the inclusion of iEF and MNI coordinates as covariates in the main TEP-amplitude models, this indicates that the diagnostic effects reported in (1)–(4) are not driven by between-group differences in stimulation parameters (Supplementary Tables 40 S, 41 S; full results in Supplementary Results (D)).

(E) Coil-to-cortex distance sensitivity analysis. All cross-sectional TEP–cognition associations identified as significant in subsection (3), P20P × diagnosis on TMT B-A after left DMN stimulation, and N20F × diagnosis on TMT B-A after both left and right ECN stimulation, survived adjustment for the site-matched coil-to-cortex distance. Variance-inflation factors were uniformly below 2 and CCD itself was non-significant or only marginally significant as a covariate. These results indicate that the reported TEP–cognition associations are not driven by atrophy-related differences in stimulation reach (Supplementary Table 42 S; full results in Supplementary Results (E)).

Discussion

This study shows that early network-targeted TEPs reveal disease-related alterations in cortical excitability within networks vulnerable to AD. Responses were hemisphere specific and linked to structural integrity and to cross-sectional and longitudinal cognitive performance. Probing cortical physiology in vivo provides a direct functional readout of how brain networks are responding to disease. This direct physiological assessment complements molecular and structural biomarkers and may help quantify brain health, track progression, and support prognosis and treatment monitoring.

DMN stimulation revealed the clearest effects. The N20F peak after stimulation left-parietal node of the DMN showed the strongest differences between groups, significantly elevated in both MCI and ADD compared to controls. The location of this response – contralateral frontal – may suggests disrupted long-distance connectivity

within the DMN. This finding aligns with the "cascading network failure" model proposed by Jones et al. (2016) [6], which posits that AD pathology spreads from posterior to anterior DMN hubs, potentially leading to compensatory or disinhibited activity in frontal areas. The asymmetry in our results, where group differences emerge after left but not right parietal stimulation, may reflect greater vulnerability of the left hemisphere in AD, consistent with imaging studies showing left-lateralized atrophy and hypometabolism in parietal regions [107–110]. Within this framework, damage to the left parietal node may impair top-down inhibitory control over the contralateral frontal cortex, resulting in an exaggerated N20F response. This pattern of posterior-to-anterior dysfunction is consistent with recent TMS-EEG findings: Ozdemir et al. (2025) [111], using source-space analysis following left-IPL stimulation in biomarker-confirmed AD, similarly reported local parietal DMN hyperexcitability and altered connectivity with frontal DMN nodes. Our bilateral, network-targeted approach extends this picture by revealing that the diagnosis-driven elevation of contralateral frontal responses is asymmetric (emerging from left but not right parietal stimulation). The left-DMN N20F effect was retained both in the fully automated peak-extraction sensitivity analysis and in the biomarker-positive subsample analyses.

The stronger diagnostic discrimination obtained from DMN than ECN stimulation likely reflects the known anatomical and temporal gradient of AD pathology i.e., the posterior DMN, and the parietal IPL in particular, is among the earliest cortical regions to accumulate amyloid-β and tau and to show functional disruption on resting-state imaging [7]. Cortical excitability changes therefore have a longer window in which to develop in DMN nodes than in frontal ECN nodes, and our network-targeted TEPs may be reflecting this pathology gradient. The elevation of contralateral frontal N20F amplitude after left parietal DMN stimulation is consistent with altered long-range propagation within the DMN, while the lateralized N20C pattern observed in the ECN may reflect a more downstream, hemispheric reorganization developing later in the disease course.

ROC analysis suggested that N20F has promising discriminatory power in distinguishing between healthy and patients, with AUC values in the fair to excellent range. Performance was lower for control versus ADD, likely because raw amplitude ROC analyses do not account for key sources of variance such as induced electric field, age, and stimulation location. When these factors were explicitly modeled in linear mixed effects analyses, robust group differences in N20F amplitude were observed after left DMN stimulation, supporting N20F as a marker of disease related alterations in cortical excitability. Future studies that minimize or standardize these sources of variance during acquisition are likely to further improve classification performance. Consistent with this, Tăuţan et al. (2023) [45] recently reported classification accuracies up to ~ 93% between AD patients and healthy controls by combining a machine-learning framework with a dense, optimized set of time-domain TEP features extracted from single-hemisphere DLPFC stimulation, illustrating the level of discrimination that TMS-EEG can reach when features are systematically optimized for the classification task. The present results complement this picture by showing that a single peak like N20F, extracted via a collapsed-localizer strategy from a network-targeted, bilateral protocol, already carries reliable group-level information, and that this signal is preserved across operator-independent peak extraction and the biomarker-positive sensitivity analysis.

After ECN stimulation, the N20C peak showed a diagnosis by hemisphere interaction. Responses were weaker in MCI than controls after left frontal stimulation and stronger in MCI and ADD after right frontal stimulation. Stronger right frontal responses in patients are, to our knowledge, novel because prior TMS-EEG work in this population has mainly targeted left prefrontal regions. The reduced left-sided N20C in MCI aligns with findings from Casarotto et al. (2011) [40], who reported diminished early TMS-evoked responses in stimulating left frontal cortex, although not targeting ECN nodes, in AD, suggesting region-specific hypoexcitability. However, this contrasts with studies such as Casula et al. (2023) [48] and Joseph et al. (2021) [46], which described increased early excitability following left DLPFC stimulation in AD. Overall, the results on the ECN, as for the DMN stimulation, are model-dependent and may reflect right frontal disinhibition linked to left frontal degeneration, consistent with patterns of interhemispheric imbalance.

ROC analyses for N20C were modest despite significant effects in mixed models, especially after left ECN stimulation. As for DMN, controlling relevant variance appears important to reveal disease related signals that are less visible in raw amplitudes.

Induced electric field strongly influenced all TEP amplitudes, with higher field strength predicting larger responses. This underscores the need to account for stimulation dose when interpreting TEP magnitude. Scaling intensity from the resting motor threshold over M1, while practical, does not guarantee comparable cortical dosing at frontal and parietal targets because excitability and scalp to cortex distance differ across regions and can be altered by atrophy and disease related physiology. Estimating and correcting for delivered field is therefore central when interpreting between group differences, and especially for clinical applications where dose must be stable across visits and comparable across patients.

TEPs showed domain specific cognitive associations distinct from structural biomarkers. Hippocampal volume and white matter integrity primarily predicted memory performance, consistent with their role in medial temporal networks [112–115], whereas TEP amplitudes were linked to executive function. In ADD, larger left DMN P20P amplitudes were associated with worse TMT B-A. P20P was strongly anticorrelated with N20C, suggesting it may reflect the complementary positive pole of a shared generator. ECN stimulation showed hemisphere dependent relationships: after left stimulation, smaller contralateral responses tended to predict better executive performance in ADD, whereas after right stimulation, better performance was associated with larger responses. This pattern suggests that the relationship between TEP amplitude and cognition is not necessarily monotonic but could potentially reflect compensatory recruitment versus disinhibition depending on hemisphere and disease stage. These results support the potential value of early TEPs for phenotyping executive vulnerability in ways not captured by structural markers. These TEP–cognition associations were retained when each focal model was re-fit with site-matched coil-to-cortex distance as an additional covariate, indicating that they are not driven by atrophy-related differences in stimulation reach. Formal joint-contributions analyses further showed that TEPs carry variance in cognitive performance that is not explained by hippocampal volume or white matter integrity.

Across studies, links between early TEPs and cognition have been inconsistent, likely due to differences in targeting, preprocessing, peak definitions, and clinical composition [43, 46, 48]. Our results support examining early contralateral as well as local peaks, and interpreting associations in a network and hemisphere specific manner rather than assuming a single direction of effect.

Early TEPs also predicted cognitive trajectories. Lower left DMN N20C amplitude at baseline predicted faster global decline on MoCA across groups over roughly 1.5 years. Although cross sectional N20C asymmetry was most evident in ADD, this longitudinal association suggests that altered local responsiveness in left parietal DMN may index vulnerability before clear group level asymmetries emerge. In the ECN, right N20C amplitude interacted with time and diagnosis in predicting executive decline: among MCI patients, larger amplitudes predicted steeper worsening, while smaller amplitudes predicted a more stable trajectory. This pattern supports hyperexcitability models in early AD [4], where excessive neuronal activity may accelerate dysfunction. Notably, N20C was not strongly tied to concurrent executive performance, suggesting it may mark latent vulnerability rather than immediate impairment. A similar pattern was observed for P20P predicting decline on ADAS cog. These longitudinal results suggest that TMS-EEG can capture a physiological vulnerability that can precede, or be partly dissociated from, current performance and structural burden.

Regarding structure, the left DMN N20C amplitude correlated with integrity of the left SLF, suggesting that WM disruption contributes to altered responses. Because this pathway links parietal and frontal DMN nodes [116], its degradation may impair within network propagation and provide a substrate for coupled changes in local and distal components. However, our tract-based approach focused on major bundles; whole brain connectivity analyses would better characterize structure function relationships and identify whether additional pathways contribute to observed TEP alterations.

In comparison, established structural biomarkers showed robust group differences and hemispheric asymmetries, consistent with prior work [6, 10, 112], but did not capture the diagnosis-by-hemisphere interactions observed in TEPs. Structural measures were strongly associated with memory but showed limited association with executive function, cross-sectionally or longitudinally. In contrast, early TEPs were linked to executive performance and decline. Together, these results suggest structural markers track staging and memory, whereas early TEPs capture physiology relevant to executive vulnerability. This multimodal comparison, together with the

formal joint-contributions analysis in which TEPs and structural markers were entered together as predictors of diagnostic group, confirms that early TEPs carry diagnostic information that is not redundant with hippocampal volume and corpus callosum mean diffusivity.

When benchmarked through ROC analysis, hippocampal volume and white matter integrity yielded the strongest discrimination between HC and patient groups. These values should however be interpreted within the design of the present study rather than as a head-to-head benchmark for TEPs. Hippocampal atrophy was part of the diagnostic inclusion criteria in this cohort, which makes its strong AUC at least partly circular when used as a diagnostic comparator. A related, more subtle caveat applies to age and education, which differ between groups partly because the recruited HC sample is younger and more educated than the patient groups, a common feature of dementia cohorts but one that inflates demographic AUCs relative to what would be obtained in a more demographically matched sample. Moreover, discrimination of MCI from ADD was substantially weaker across all structural and demographic measures, indicating that these markers separate clinically established dementia from controls more readily than they track within-disease progression. Beyond benchmarking, we also examined whether TEPs and structural biomarkers carry overlapping or independent information about cognition and diagnosis: cross-sectionally, the two sets of markers predicted different cognitive domains (executive function for TEPs, memory and global cognition for structural markers); longitudinally, baseline TEPs retained independent prognostic value for cognitive decline once hippocampal volume was included in the model; and for diagnostic classification the most informative TEP component added discriminatory power above structural markers, while these reciprocally added information above the TEP. More generally, hippocampal volume, white matter integrity, and TEPs are not interchangeable markers competing for a single diagnostic role. Rather, they index different aspects of the disease process i.e., structural measures capture downstream neurodegeneration, whereas early TEPs probe ongoing cortical physiology, and none of them, on its own, indexes AD pathology in the molecular sense, which would require amyloid or tau measures. The aim of the present work is not to propose TEPs as a stand-alone diagnostic test, but to establish that early network-targeted TEPs carry disease-related information across the AD spectrum, as a first step toward their more relevant potential applications in prognosis and treatment monitoring.

Limitations

Several steps can strengthen clinical interpretability and generalizability. Future studies should recruit biomarker defined cohorts using harmonized panels (for example cerebrospinal fluid, PET, genetics, and blood markers) to link pathological profiles to TEP patterns. Larger multicenter samples with broader demographic representation, together with harmonized acquisition and preprocessing, will improve power, generalizability, and reproducibility. Individualized electric field modeling should calibrate stimulation intensity to ensure comparable dosing across regions, atrophy levels, and visits. Network targeting can be refined by integrating multimodal indices of regional vulnerability to optimize site selection and test more specific network hypotheses. Finally, source reconstructed TEPs can help identify generators of early components and support integration with multimodal imaging. The longitudinal subsample ($n = 55$) is smaller than baseline, with the most pronounced attrition in the MCI group (27 → 10 participants). Several factors contributed to this pattern, including the timing of re-contact and re-assessment during and after the COVID-19 pandemic, which disproportionately affected access to clinical research visits for older and cognitively vulnerable participants. The within-subject mixed-effects models used here partial out time-invariant subject variance and remain unbiased under a missing-at-random assumption conditional on baseline diagnosis and demographics, and the omnibus analysis of group-level cognitive trajectories confirms that the expected pattern of decline is recoverable in the retained sample. Nonetheless, residual selective attrition cannot be excluded. For example, more clinically progressed MCI participants being more likely to drop out, which would bias the longitudinal slope estimates toward shallower decline and make our prognostic findings conservative

rather than inflated. The longitudinal results should therefore be interpreted as conditional on the follow-up subsample we were able to retest, with replication in larger, prospectively designed cohorts needed to confirm and extend the prognostic value of these early TEP measures. Although a fully automated, operator-independent peak-extraction pipeline was used as a sensitivity analysis (Supplementary Results (B)) and confirmed the principal findings, the inter-rater reliability of the semi-automated peak extraction used in the main analyses was not formally quantified across multiple raters in the present cohort; future work should systematically test this reproducibility.

Finally, the mechanistic interpretations advanced in this study, including compensatory hyperexcitability, loss of inhibitory control, and interhemispheric imbalance, are presented as candidate accounts consistent with the present findings and with the existing TMS–EEG and AD literature, rather than as claims directly tested in this study. The present design quantifies group differences and brain-cognition relationships in TEP amplitude; the cellular and circuit-level mechanisms underlying these signatures will require targeted experimental probes (e.g., paired-pulse paradigms, pharmacological interactions of GABAergic and glutamatergic neurotransmission, combined TMS–EEG–imaging acquisitions) and were not the focus of the present work.

Conclusions

Network targeted TMS EEG reveals hemisphere and network specific excitability changes across the AD spectrum. Early TEP components, particularly N20F after left parietal DMN stimulation, differentiated MCI and ADD from controls, while ECN responses showed lateralized patterns consistent with interhemispheric imbalance. Early TEPs related to executive function and predicted cognitive decline in ways partly distinct from structural biomarkers. With improved dose calibration and targeting, early network targeted TEPs may complement molecular and structural measures for monitoring physiological disease impact and interventions.

Abbreviations

AD	Alzheimer's disease
ADD	Alzheimer's disease dementia
ADAS-cog	Alzheimer's Disease Assessment Scale-Cognitive Subscale
AUC	Area under the curve
CSF	Cerebrospinal fluid
DLPFC	Dorsolateral prefrontal cortex
DMN	Default mode network
DWI	Diffusion-weighted imaging
ECN	Executive control network
EEG	Electroencephalography
FA	Fractional anisotropy
FDG-PET	Fluorodeoxyglucose positron emission tomography
FDI	First dorsal interosseous
gCC	Genu of the corpus callosum
HC	Healthy controls
IPL	Inferior parietal lobule
IQR	Interquartile range
LMM	Linear mixed model
MCI	Mild cognitive impairment
MD	Mean diffusivity
MEP	Motor-evoked potential

MMSE	Mini-Mental State Examination
MNI	Montreal Neurological Institute
MoCA	Montreal Cognitive Assessment
MRI	Magnetic resonance imaging
RAVLT	Rey Auditory Verbal Learning Test
rMT	Resting motor threshold
ROC	Receiver operating characteristic
ROI	Region of interest
sCC	Splenium of the corpus callosum
SLF	Superior longitudinal fasciculus
TEP	TMS-evoked potential
TMS	Transcranial magnetic stimulation
TMT	Trail Making Test

Supplementary Information The online version contains supplementary material available at https://doi.org/10.1186/s13195-026-02176-4.

Acknowledgements We are grateful to all participants and their families for their time and commitment to this study, particularly given the logistical challenges posed by the COVID-19 pandemic. We also thank the research staff and collaborators who contributed to data collection and study coordination but do not meet authorship criteria.

Authors' contributions GB collected and processed TMS–EEG data, performed statistical analyses, wrote the manuscript, prepared figures, and managed all revisions. EC contributed to study conceptualization, MRI data acquisition, network-based stimulation site selection, and manuscript revision. CB contributed to neuropsychological data collection and analysis. FF contributed to MRI data acquisition and processing. NSB provided statistical consultancy. DB secured funding, provided scientific consultancy, and revised the manuscript. MBu contributed to neuropsychological data collection and analysis. VC contributed to MRI data acquisition and processing. MD contributed to neuropsychological data collection and analysis. EF contributed to neuropsychological data collection and analysis. CF contributed to TMS–EEG data collection and laboratory management. PJF contributed to manuscript revision and funding acquisition. DL contributed to TMS–EEG data collection. EM contributed to TMS–EEG data collection. MM contributed to hippocampal volume analysis. AC contributed to hippocampal volume analysis. VN contributed to neuropsychological data collection. GQ contributed to hippocampal volume analysis and network-based stimulation site selection. SS contributed to neuropsychological data collection. MP contributed to study conceptualization, MRI data acquisition, network-based stimulation site selection, and manuscript revision. VR revised the manuscript. AS contributed to TMS–EEG data preprocessing. MF secured funding. FA secured funding, co-supervised the study, and revised the manuscript. MB conceived and supervised the study as principal investigator, secured funding, and revised the manuscript. All authors read and approved the final manuscript.

Funding This work was supported by the IRCCS Istituto Centro San Giovanni di Dio Fatebenefratelli in Brescia, partially supported by the Italian Ministry of Health (Ricerca Corrente); Bando della ricerca finalizzata 2016 – Giovani Ricercatori (grant no: GR-2016-02364132).

Data availability The data that support the findings of this study will be published on NeuGRID2 (https://www.neugrid2.eu/).

Declarations

Ethics approval and consent to participate All procedures were performed according to the Declaration of Helsinki. The study protocol was approved by the local ethical standards committee on human experimentation at IRCCS Istituto Centro San Giovanni di Dio Fatebenefratelli, Brescia, Italy (approval no: 33/2018). Written informed consent was obtained from participants with capacity to consent, or from their legally authorized representatives when capacity was lacking. In these cases, study procedures were also explained to participants in simple terms, and participation proceeded only if they showed no signs of distress or unwillingness.

Consent for publication Not applicable.

Competing interests The authors declare no competing interests.

Open Access This article is licensed under a Creative Commons Attribution 4.0 International License, which permits use, sharing, adaptation, distribution and reproduction in any medium or format, as long as you give appropriate credit to the original author(s) and the source, provide a link to the Creative Commons licence, and indicate if changes were made. The images or other third party material in this article are included in the article's Creative Commons licence, unless indicated otherwise in a credit line to the material. If material is not included in the article's Creative Commons licence and your intended use is not permitted by statutory regulation or exceeds the permitted use, you will need to obtain permission directly from the copyright holder. To view a copy of this licence, visit http://creativecommons.org/licenses/by/4.0/.

References

1. Kukull WA, Bowen JD. Dementia epidemiology. The Medical clinics of North America. Med Clin North Am. 2002;86:573–90. https://doi.org/10.1016/S0025-7125(02)00010-X.
2. Prince M, Albanese E, Pender R, Ferri C, Mazzotti DR, Piovezan RD et al. World Alzheimer Report 2014: Dementia and risk reduction: An analysis of protective and modifiable risk factors. 2014. Cited 2022 Dec 17. https://www.alzint.org/resource/world-alzheimer-report-2014/. Accessed 17 Dec 2022.
3. De Strooper B, Karran E. The Cellular Phase of Alzheimer's Disease. Cell Cell. 2016;164:603–15. https://doi.org/10.1016/J.CELL.2015.12.056.
4. Palop JJ, Mucke L. Network abnormalities and interneuron dysfunction in Alzheimer disease. Nat reviews Neurosci Nat Rev Neurosci. 2016;17:777–92. https://doi.org/10.1038/NRN.2016.141.
5. Sperling R. Potential of functional MRI as a biomarker in early Alzheimer's disease. Neurobiology of aging. Neurobiol Aging. 2011;32:Suppl 1. https://doi.org/10.1016/J.NEUROBIOLAGING.2011.09.009. Cited 2022 Dec 17.
6. Jones DT, Knopman DS, Gunter JL, Graff-Radford J, Vemuri P, Boeve BF, et al. Cascading network failure across the Alzheimer's disease spectrum. Brain Oxf Acad. 2016;139:547–62. https://doi.org/10.1093/BRAIN/AWV338.
7. Palmqvist S, Schöll M, Strandberg O, Mattsson N, Stomrud E, Zetterberg H et al. Earliest accumulation of β-amyloid occurs within the default-mode network and concurrently affects brain connectivity. Nature communications. Nat Commun. 2017;8. https://doi.org/10.1038/S41467-017-01150-X. Cited 2021 Nov 17.
8. Brier MR, Thomas JB, Snyder AZ, Benzinger TL, Zhang D, Raichle ME, et al. Loss of intranetwork and internetwork resting state functional connections with Alzheimer's disease progression. J Neurosci. 2012;32:8890–9. https://doi.org/10.1523/JNEUROSCI.5698-11.2012.
9. Soman SM, Raghavan S, Rajesh PG, Mohanan N, Thomas B, Kesavadas C, et al. Does resting state functional connectivity differ between mild cognitive impairment and early Alzheimer's dementia? Journal of the Neurological Sciences. Elsevier B.V. 2020;418. https://doi.org/10.1016/j.jns.2020.117093. Cited 2022 Dec 17.
10. Filippi M, Basaia S, Canu E, Imperiale F, Magnani G, Falautano M, et al. Changes in functional and structural brain connectome along the Alzheimer's disease continuum. Mol psychiatry Mol Psychiatry. 2020;25:230–9. https://doi.org/10.1038/S41380-018-0067-8.
11. Canu E, Agosta F, Spinelli EG, Magnani G, Marcone A, Scola E, et al. White matter microstructural damage in Alzheimer's disease at different ages of onset. Neurobiol aging Neurobiol Aging. 2013;34:2331–40. https://doi.org/10.1016/J.NEUROBIOLAGING.2013.03.026.
12. Grande G, Valletta M, Rizzuto D, Xia X, Qiu C, Orsini N, et al. Blood-based biomarkers of Alzheimer's disease and incident dementia in the community. Nat Med Nat Publishing Group. 2025;31:2027–35. https://doi.org/10.1038/s41591-025-03605-x.
13. Schöll M, Verberk IMW, Del Campo M, Delaby C, Therriault J, Chong JR, et al. Challenges in the practical implementation of blood biomarkers for Alzheimer's disease. Lancet Healthy Longev. 2024;5:100630. https://doi.org/10.1016/j.lanhl.2024.07.013.
14. Ossenkoppele R, Pichet Binette A, Groot C, Smith R, Strandberg O, Palmqvist S, et al. Amyloid and tau PET-positive cognitively unimpaired individuals are at high risk for future cognitive decline. Nat Med. 2022;28:2381–7. https://doi.org/10.1038/s41591-022-02049-x.
15. Jack CR, Bennett DA, Blennow K, Carrillo MC, Dunn B, Haeberlein SB, et al. NIA-AA Research Framework: Toward a biological definition of Alzheimer's disease. Alzheimer's & dementia: the journal of the Alzheimer's Association. Alzheimers Dement. 2018;14:535–62. https://doi.org/10.1016/J.JALZ.2018.02.018.
16. Jack CR, Holtzman DM. Biomarker Modeling of Alzheimer's Disease. Neuron. 2013;80:1347–58. https://doi.org/10.1016/j.neuron.2013.12.003.
17. Rangaprakash D, Barry RL, Deshpande G. The confound of hemodynamic response function variability in human resting-state functional MRI studies. Front Neurosci. 2023;17:934138. https://doi.org/10.3389/fnins.2023.934138.

18. Tagamets M-A, Horwitz B. Interpreting PET and fMRI measures of functional neural activity: the effects of synaptic inhibition on cortical activation in human imaging studies. Brain Res Bull. 2001;54:267–73. https://doi.org/10.1016/S0361-9230(00)00435-4.
19. Babiloni C, Arakaki X, Azami H, Bennys K, Blinowska K, Bonanni L, et al. Measures of resting state EEG rhythms for clinical trials in Alzheimer's disease: Recommendations of an expert panel. Alzheimer's Dement. 2021;17:1528–53. https://doi.org/10.1002/alz.12311.
20. Cassani R, Estarellas M, San-Martin R, Fraga FJ, Falk TH. Systematic Review on Resting-State EEG for Alzheimer's Disease Diagnosis and Progression Assessment. Dis Markers. 2018;2018:1–26. https://doi.org/10.1155/2018/5174815.
21. Hallett M. Transcranial Magnetic Stimulation: A Primer. Neuron. 2007;55:187–99. https://doi.org/10.1016/j.neuron.2007.06.026.
22. Rossini PM, Burke D, Chen R, Cohen LG, Daskalakis Z, Di Iorio R, et al. Non-invasive electrical and magnetic stimulation of the brain, spinal cord, roots and peripheral nerves: Basic principles and procedures for routine clinical and research application: An updated report from an I.F.C.N. Committee. Clin Neurophysiol Elsevier. 2015;126:1071–107. https://doi.org/10.1016/j.clinph.2015.02.001.
23. Barker AT, Jalinous R, Freeston IL. Non-invasive magnetic stimulation of human cortex. Lancet. 1985;325:1106–7.
24. Bradley C, Nydam AS, Dux PE, Mattingley JB. State-dependent effects of neural stimulation on brain function and cognition. Nat Rev Neurosci. 2022;23:459–75. https://doi.org/10.1038/s41583-022-00598-1.
25. Caulfield KA, Li X, George MS. Four electric field modeling methods of Dosing Prefrontal Transcranial Magnetic Stimulation (TMS): Introducing APEX MT dosimetry. Brain Stimul. 2021;14:1032–4. https://doi.org/10.1016/j.brs.2021.06.012.
26. Caulfield KA, Fleischmann HH, Cox CE, Wolf JP, George MS, McTeague LM. Neuronavigation maximizes accuracy and precision in TMS positioning: Evidence from 11,230 distance, angle, and electric field modeling measurements. Brain Stimul. 2022;15:1192–205. https://doi.org/10.1016/j.brs.2022.08.013.
27. He H, Sun X, Doose J, Faller J, McIntosh JR, Saber GT, et al. TMS-induced modulation of brain networks and its associations to rTMS treatment for depression: a concurrent fMRI-EEG-TMS study. Brain Stimul. 2025;18:1955–65. https://doi.org/10.1016/j.brs.2025.10.013.
28. Miniussi C, Bortoletto M. Harnessing neural variability: Implications for brain research and non-invasive brain stimulation. Neurosci Biobehavioral Reviews. 2025;176:106312. https://doi.org/10.1016/j.neubiorev.2025.106312.
29. Thielscher A, Opitz A, Windhoff M. Impact of the gyral geometry on the electric field induced by transcranial magnetic stimulation. NeuroImage Acad Press. 2011;54:234–43. https://doi.org/10.1016/J.NEUROIMAGE.2010.07.061.
30. Ilmoniemi RJ, Kičić D. Methodology for combined TMS and EEG. Brain Topogr. 2010;22:233–48. https://doi.org/10.1007/s10548-009-0123-4.
31. Bortoletto M, Veniero D, Thut G, Miniussi C. The contribution of TMS-EEG coregistration in the exploration of the human cortical connectome. Neurosci Biobehav Rev. 2015;49:114–24. https://doi.org/10.1016/j.neubiorev.2014.12.014.
32. Tremblay S, Rogasch NC, Premoli I, Blumberger DM, Casarotto S, Chen R, et al. Clinical utility and prospective of TMS–EEG. Clinical Neurophysiology. Elsevier Irel Ltd. 2019;130:802–44. https://doi.org/10.1016/j.clinph.2019.01.001.
33. Julkunen P, Kimiskidis VK, Belardinelli P. Bridging the gap: TMS-EEG from lab to clinic. J Neurosci Methods Elsevier. 2022;369:109482. https://doi.org/10.1016/J.JNEUMETH.2022.109482.
34. Massimini M, Boly M, Casali A, Rosanova M, Tononi G. A perturbational approach for evaluating the brain's capacity for consciousness. Progress in Brain Research. Elsevier. 2009;201–14. https://doi.org/10.1016/S0079-6123(09)17714-2. Cited 2026 May 11.
35. Casarotto S, Comanducci A, Rosanova M, Sarasso S, Fecchio M, Napolitani M, et al. Stratification of unresponsive patients by an independently validated index of brain complexity. Annals of neurology. Ann Neurol. 2016;80:718–29. https://doi.org/10.1002/ANA.24779.
36. Pievani M, De Haan W, Wu T, Seeley WW, Frisoni GB. Functional network disruption in the degenerative dementias. Lancet Neurol. 2011;10:829–43. https://doi.org/10.1016/S1474-4422(11)70158-2.
37. Nakamura A, Cuesta P, Kato T, Arahata Y, Iwata K, Yamagishi M, et al. Early functional network alterations in asymptomatic elders at risk for Alzheimer's disease. Sci Rep Nat Publishing Group. 2017;7:6517. https://doi.org/10.1038/s41598-017-06876-8.
38. Julkunen P, Jauhiainen AM, Westerén-Punnonen S, Pirinen E, Soininen H, Könönen M, et al. Navigated TMS combined with EEG in mild cognitive impairment and Alzheimer's disease: A pilot study. J Neurosci Methods Elsevier. 2008;172:270–6. https://doi.org/10.1016/J.JNEUMETH.2008.04.021.
39. Julkunen P, Jauhiainen AM, Könönen M, Pääkkönen A, Karhu J, Soininen H. Combining Transcranial Magnetic Stimulation and Electroencephalography May Contribute to Assess the Severity of Alzheimer's Disease. Int J Alzheimer's Disease. 2011;2011:1–9. https://doi.org/10.4061/2011/654794.
40. Casarotto S, Määttä S, Herukka SK, Pigorini A, Napolitani M, Gosseries O, et al. Transcranial magnetic stimulation-evoked EEG/cortical potentials in physiological and pathological aging. NeuroReport. 2011;22:592–7. https://doi.org/10.1097/WNR.0B013E328349433A.

41. Zifman N, Levy-Lamdan O, Suzin G, Efrati S, Tanne D, Fogel H, et al. Introducing a Novel Approach for Evaluation and Monitoring of Brain Health Across Life Span Using Direct Non-invasive Brain Network Electrophysiology. Front Aging Neurosci. 2019;11:248. https://doi.org/10.3389/fnagi.2019.00248.
42. Ferreri F, Guerra A, Vollero L, Ponzo D, Määttä S, Könönen M et al. TMS-EEG Biomarkers of Amnestic Mild Cognitive Impairment Due to Alzheimer's Disease: A Proof-of-Concept Six Years Prospective Study. Frontiers in aging neuroscience. Front Aging Neurosci. 2021;13. https://doi.org/10.3389/FNAGI.2021.737281. Cited 2022 Sept 27.
43. Bagattini C, Mutanen TP, Fracassi C, Manenti R, Cotelli M, Ilmoniemi RJ, et al. Predicting Alzheimer's disease severity by means of TMS–EEG coregistration. Neurobiol Aging Elsevier Inc. 2019;80:38–45. https://doi.org/10.1016/j.neurobiolaging.2019.04.008.
44. Ferreri F, Vecchio F, Vollero L, Guerra A, Petrichella S, Ponzo D, et al. Sensorimotor cortex excitability and connectivity in Alzheimer's disease: A TMS-EEG Co-registration study. Hum Brain Mapp John Wiley Sons Inc. 2016;37:2083–96. https://doi.org/10.1002/hbm.23158.
45. Tăuţan A-M, Casula EP, Pellicciari MC, Borghi I, Maiella M, Bonni S, et al. TMS-EEG perturbation biomarkers for Alzheimer's disease patients classification. Sci Rep. 2023;13:7667. https://doi.org/10.1038/s41598-022-22978-4.
46. Joseph S, Knezevic D, Zomorrodi R, Blumberger DM, Daskalakis ZJ, Mulsant BH, et al. Dorsolateral prefrontal cortex excitability abnormalities in Alzheimer's Dementia: Findings from transcranial magnetic stimulation and electroencephalography study. Int J Psychophysiol. 2021;169:55–62. https://doi.org/10.1016/j.ijpsycho.2021.08.008.
47. Zhang J, Lu H, Zhu L, Ren H, Dang G, Su X, et al. Classification of Cognitive Impairment and Healthy Controls Based on Transcranial Magnetic Stimulation Evoked Potentials. Front Aging Neurosci. 2021;13:804384. https://doi.org/10.3389/fnagi.2021.804384.
48. Casula EP, Borghi I, Maiella M, Pellicciari MC, Bonnì S, Mencarelli L, et al. Regional Precuneus Cortical Hyperexcitability in Alzheimer's Disease Patients. Ann Neurol. 2023;93:371–83. https://doi.org/10.1002/ana.26514.
49. Lin H, Liang J, Wang Q, Shao Y, Song P, Li S, et al. Effects of accelerated intermittent theta-burst stimulation in modulating brain of Alzheimer's disease. Cereb Cortex. 2024;34:bhae106. https://doi.org/10.1093/cercor/bhae106.
50. Maiella M, Mencarelli L, Casula EP, Borghi I, Assogna M, di Lorenzo F, et al. Breakdown of TMS evoked EEG signal propagation within the default mode network in Alzheimer's disease. Clin Neurophysiol. 2024;167:177–88. https://doi.org/10.1016/j.clinph.2024.09.007.
51. Casula EP, Pellicciari MC, Bonnì S, Borghi I, Maiella M, Assogna M, et al. Decreased Frontal Gamma Activity in Alzheimer Disease Patients. Ann Neurol. 2022;92:464–75. https://doi.org/10.1002/ana.26444.
52. Huntley J, Bor D, Deng F, Mancuso M, Mediano PAM, Naci L et al. Assessing awareness in severe Alzheimer's disease. Frontiers in Human Neuroscience. 2023 [Cited 2024 Mar 1];16. https://www.frontiersin.org/articles/ https://doi.org/10.3389/fnhum.2022.1035195. Accessed 1 Mar 2024.
53. Koch G, Bonnì S, Pellicciari MC, Casula EP, Mancini M, Esposito R, et al. Transcranial magnetic stimulation of the precuneus enhances memory and neural activity in prodromal Alzheimer's disease. NeuroImage Acad Press. 2018;169:302–11. https://doi.org/10.1016/J.NEUROIMAGE.2017.12.048.
54. Koch G, Casula EP, Bonnì S, Borghi I, Assogna M, Minei M, et al. Precuneus magnetic stimulation for Alzheimer's disease: a randomized, sham-controlled trial. Brain. 2022;145:3776–86. https://doi.org/10.1093/brain/awac285.
55. Liu C, Han T, Xu Z, Liu J, Zhang M, Du J, et al. Modulating Gamma Oscillations Promotes Brain Connectivity to Improve Cognitive Impairment. Cereb Cortex. 2022;32:2644–56. https://doi.org/10.1093/cercor/bhab371.
56. Koch G, Motta C, Bonnì S, Pellicciari MC, Picazio S, Casula EP, et al. Effect of Rotigotine vs Placebo on Cognitive Functions Among Patients With Mild to Moderate Alzheimer Disease: A Randomized Clinical Trial. JAMA Netw Open. 2020;3:e2010372. https://doi.org/10.1001/jamanetworkopen.2020.10372.
57. Bagattini C, Brignani D, Bonnì S, Quattrini G, Gasparotti R, Pievani M. Functional Imaging to Guide Network-Based TMS Treatments: Toward a Tailored Medicine Approach in Alzheimer's Disease. Front Neurosci. 2021;15:687493. https://doi.org/10.3389/fnins.2021.687493.
58. McKhann GM, Knopman DS, Chertkow H, Hyman BT, Jack CR, Kawas CH, et al. The diagnosis of dementia due to Alzheimer's disease: recommendations from the National Institute on Aging-Alzheimer's Association workgroups on diagnostic guidelines for Alzheimer's disease. Alzheimer's dementia: J Alzheimer's Association Alzheimers Dement. 2011;7:263–9. https://doi.org/10.1016/J.JALZ.2011.03.005.
59. Albert MS, DeKosky ST, Dickson D, Dubois B, Feldman HH, Fox NC, et al. The diagnosis of mild cognitive impairment due to Alzheimer's disease: Recommendations from the National Institute on Aging-Alzheimer's Association workgroups on diagnostic guidelines for Alzheimer's disease. Alzheimer's Dement. 2011;7:270–9. https://doi.org/10.1016/j.jalz.2011.03.008.
60. Rossi S, Hallett M, Rossini PM, Pascual-Leone A. Safety of TMS Consensus Group TS of TC. Safety, ethical considerations, and application guidelines for the use of transcranial magnetic stimulation in clinical practice and research. Clin neurophysiology: official J Int Federation Clin Neurophysiol NIH Public Access. 2009;120:2008–39. https://doi.org/10.1016/j.clinph.2009.08.016.
61. Sammet S, New York LLC. 2016;41:444–51. https://doi.org/10.1007/s00261-016-0680-4.

62. Awiszus F. On relative frequency estimation of transcranial magnetic stimulation motor threshold. Clinical neurophysiology: official journal of the International Federation of Clinical Neurophysiology. Clin Neurophysiol. 2012;123:2319–20. https://doi.org/10.1016/J.CLINPH.2012.04.014.
63. Awiszus F. Fast estimation of transcranial magnetic stimulation motor threshold: Is it safe? Brain Stimulation. Elsevier Inc. 2011;4:50–7. https://doi.org/10.1016/j.brs.2010.06.002.
64. Awiszus F. TMS and threshold hunting. Supplements to Clinical neurophysiology. Suppl Clin Neurophysiol. 2003;56:13–23. https://doi.org/10.1016/S1567-424X(09)70205-3.
65. Rothwell JC, Hallett M, Berardelli A, Eisen A, Rossini P, Paulus W. Magnetic stimulation: motor evoked potentials. The International Federation of Clinical Neurophysiology. Electroencephalogr Clin Neurophysiol Suppl. 1999;52:97–103.
66. Dissanayaka T, Zoghi M, Farrell M, Egan G, Jaberzadeh S. Comparison of Rossini-Rothwell and adaptive threshold-hunting methods on the stability of TMS induced motor evoked potentials amplitudes. J Neurosci Res J Neurosci Res. 2018;96:1758–65. https://doi.org/10.1002/JNR.24319.
67. Shirer WR, Ryali S, Rykhlevskaia E, Menon V, Greicius MD. Decoding Subject-Driven Cognitive States with Whole-Brain Connectivity Patterns. Cereb Cortex Oxf Acad. 2012;22:158–65. https://doi.org/10.1093/CERCOR/BHR099.
68. Greene SJ, Killiany RJ. Subregions of the inferior parietal lobule are affected in the progression to Alzheimer's disease. Neurobiol Aging. 2010;31:1304–11. https://doi.org/10.1016/j.neurobiolaging.2010.04.026.
69. Greicius MD, Srivastava G, Reiss AL, Menon V. Default-mode network activity distinguishes Alzheimer's disease from healthy aging: evidence from functional MRI. Proc Natl Acad Sci U S A. 2004;101:4637–42. https://doi.org/10.1073/pnas.0308627101.
70. Grieder M, Wang DJJ, Dierks T, Wahlund L-O, Jann K. Default Mode Network Complexity and Cognitive Decline in Mild Alzheimer's Disease. Front Neurosci. 2018;12:770. https://doi.org/10.3389/fnins.2018.00770.
71. Yuan Q, Qi W, Xue C, Ge H, Hu G, Chen S, et al. Convergent Functional Changes of Default Mode Network in Mild Cognitive Impairment Using Activation Likelihood Estimation. Front Aging Neurosci. 2021;13:708687. https://doi.org/10.3389/fnagi.2021.708687.
72. Daigle KM, Pietrzykowski MO, Waters AB, Swenson LP, Gansler DA. Central Executive Network and Executive Function in Patients With Alzheimer's Disease and Healthy Individuals: Meta-Analysis of Structural and Functional MRI. JNP. 2022;34:204–13. https://doi.org/10.1176/appi.neuropsych.20110279.
73. Kumar S, Zomorrodi R, Ghazala Z, Goodman MS, Blumberger DM, Cheam A, et al. Extent of Dorsolateral Prefrontal Cortex Plasticity and Its Association With Working Memory in Patients With Alzheimer Disease. JAMA Psychiatry Am Med Association. 2017;74:1266–74. https://doi.org/10.1001/JAMAPSYCHIATRY.2017.3292.
74. Jones DT, Graff-Radford J. Executive Dysfunction and the Prefrontal Cortex. Continuum. 2021;27:1586–601. https://doi.org/10.1212/CON.0000000000001009.
75. Conde V, Tomasevic L, Akopian I, Stanek K, Saturnino GB, Thielscher A, et al. The non-transcranial TMS-evoked potential is an inherent source of ambiguity in TMS-EEG studies. NeuroImage Acad Press Inc. 2019;185:300–12. https://doi.org/10.1016/j.neuroimage.2018.10.052.
76. Belardinelli P, Biabani M, Blumberger DM, Bortoletto M, Casarotto S, David O, et al. Reproducibility in TMS–EEG studies: A call for data sharing, standard procedures and effective experimental control. Brain Stimulation Elsevier Inc. 2019;12:787–90. https://doi.org/10.1016/j.brs.2019.01.010.
77. Rocchi L, Di Santo A, Brown K, Ibáñez J, Casula E, Rawji V, et al. Disentangling EEG responses to TMS due to cortical and peripheral activations. Brain Stimulation Elsevier Inc. 2021;14:4–18. https://doi.org/10.1016/j.brs.2020.10.011.
78. Hernandez-Pavon JC, Veniero D, Bergmann TO, Belardinelli P, Bortoletto M, Casarotto S, et al. TMS combined with EEG: Recommendations and open issues for data collection and analysis. Brain Stimul. 2023;16:567–93. https://doi.org/10.1016/j.brs.2023.02.009.
79. Mutanen TP, Metsomaa J, Liljander S, Ilmoniemi RJ. Automatic and robust noise suppression in EEG and MEG: The SOUND algorithm. NeuroImage. 2018;166:135–51. https://doi.org/10.1016/j.neuroimage.2017.10.021.
80. Mutanen TP, Kukkonen M, Nieminen JO, Stenroos M, Sarvas J, Ilmoniemi RJ. Recovering TMS-evoked EEG responses masked by muscle artifacts. NeuroImage Acad Press Inc. 2016;139:157–66. https://doi.org/10.1016/j.neuroimage.2016.05.028.
81. Luck SJ. An introduction to the event-related potential technique. MIT Press; 2014.
82. Folstein MF, Folstein SE, McHugh PR. Mini-mental state. J Psychiatr Res. 1975;12:189–98. https://doi.org/10.1016/0022-3956(75)90026-6.
83. Conti S, Bonazzi S, Laiacona M, Masina M, Coralli MV. Montreal Cognitive Assessment (MoCA)-Italian version: regression based norms and equivalent scores. Neurol Sci. 2015;36:209–14. https://doi.org/10.1007/s10072-014-1921-3.
84. Fioravanti M. ADAS –Alzheimer's Disease Assessment Scale.· versione italiana. Firenze: Giunti Organizzazioni Speciali; 1996.
85. Kueper JK, Speechley M, Montero-Odasso M. The Alzheimer's Disease Assessment Scale–Cognitive Subscale (ADAS-Cog): Modifications and Responsiveness in Pre-Dementia Populations. Narrative Rev J Alzheimer's Disease. 2018;63:423–44. https://doi.org/10.3233/JAD-170991.

86. Carlesimo GA, Caltagirone C, Gainotti G. The Mental Deterioration Battery: normative data, diagnostic reliability and qualitative analyses of cognitive impairment. The Group for the Standardization of the Mental Deterioration Battery. Volume 36. Switzerland: European neurology; 1996. pp. 378–84.
87. Frasson P, Ghiretti R, Catricalà E, Pomati S, Marcone A, Parisi L, et al. Free and cued selective reminding test: an Italian normative study. Neurol Sci. 2011;32:1057–62. https://doi.org/10.1007/s10072-011-0607-3.
88. Monaco M, Costa A, Caltagirone C, Carlesimo GA. Forward and backward span for verbal and visuo-spatial data: standardization and normative data from an Italian adult population.. Neurol Sci. 2013;34:749–54. https://doi.org/10.1007/s10072-012-1130-x.
89. Monaco M, Costa A, Caltagirone C, Carlesimo GA. Erratum to: Forward and backward span for verbal and visuo-spatial data: standardization and normative data from an Italian adult population. Neurol Sci. 2015;36:345–7. https://doi.org/10.1007/s10072-014-2019-7.
90. Caffarra P, Vezzadini G, Dieci F, Zonato F, Venneri A. Rey-Osterrieth complex figure: normative values in an Italian population sample. Neurol Sci. 2002;22:443–7. https://doi.org/10.1007/s100720200003.
91. Novelli G, Papagno C, Capitani E, Laiacona M, et al. Tre test clinici di ricerca e produzione lessicale. Taratura su sogetti normali. [Three clinical tests to research and rate the lexical performance of normal subjects]. Archivio di Psicologia Neurologia e Psichiatria. 1986;47:477–506.
92. Giovagnoli AR, Del Pesce M, Mascheroni S, Simoncelli M, Laiacona M, Capitani E. Trail making test: normative values from 287 normal adult controls. Ital J Neuro Sci. 1996;17:305–9. https://doi.org/10.1007/BF01997792.
93. Della Sala S, Laiacona M, Spinnler H, Ubezio C. A cancellation test: its reliability in assessing attentional deficits in Alzheimer's disease. Psychol Med. 1992;22:885–901. https://doi.org/10.1017/S0033291700038460.
94. Caffarra P, Vezzadini G, Dieci F, Zonato F, Venneri A. Una versione abbreviata del test di Stroop: dati normativi nella popolazione italiana. Nuova rivista di neurologia. Pensiero Scientifico. 2002;12:111–5.
95. Basso A, Capitani E, Laiacona M. Raven's coloured progressive matrices: normative values on 305 adult normal controls. Funct Neurol. 1987;2:189–94.
96. Yesavage JA, Brink TL, Rose TL, Lum O, Huang V, Adey M, et al. Development and validation of a geriatric depression screening scale: A preliminary report. J Psychiatr Res. 1982;17:37–49. https://doi.org/10.1016/0022-3956(82)90033-4.
97. Lezak MD, Howieson DB, Bigler ED, Tranel D. Neuropsychological assessment. 5th ed. Oxford University Press; 2012.
98. Andrews-Hanna JR, Reidler JS, Sepulcre J, Poulin R, Buckner RL. Functional-Anatomic Fractionation of the Brain's Default Network. Neuron. 2010;65:550–62. https://doi.org/10.1016/j.neuron.2010.02.005.
99. Buckner RL, Andrews-Hanna JR, Schacter DL. The Brain's Default Network Anatomy, Function, and Relevance to Disease. Ann N Y Acad Sci. 2008;1124:1–38. https://doi.org/10.1196/annals.1440.011.
100. Niendam TA, Laird AR, Ray KL, Dean YM, Glahn DC, Carter CS. Meta-analytic evidence for a superordinate cognitive control network subserving diverse executive functions. Cogn Affect Behav Neurosci. 2012;12:241–68. https://doi.org/10.3758/s13415-011-0083-5.
101. Menon V, D'Esposito M. The role of PFC networks in cognitive control and executive function. Neuropsychopharmacol. 2022;47:90–103. https://doi.org/10.1038/s41386-021-01152-w.
102. Spreng RN, Stevens WD, Chamberlain JP, Gilmore AW, Schacter DL. Default network activity, coupled with the frontoparietal control network, supports goal-directed cognition. NeuroImage. 2010;53:303–17. https://doi.org/10.1016/j.neuroimage.2010.06.016.
103. Crittenden BM, Mitchell DJ, Duncan J. Recruitment of the default mode network during a demanding act of executive control. eLife. 2015;4:e06481. https://doi.org/10.7554/eLife.06481.
104. Mevel K, Chételat G, Eustache F, Desgranges B. The Default Mode Network in Healthy Aging and Alzheimer′s Disease. Urakami K, editor. International Journal of Alzheimer's Disease. 2011;2011:535816. https://doi.org/10.4061/2011/535816.
105. Wang L, Li H, Liang Y, Zhang J, Li X, Shu N, et al. Amnestic Mild Cognitive Impairment: Topological Reorganization of the Default-Mode Network. Radiology. 2013;268:501–14. https://doi.org/10.1148/radiol.13121573.
106. Fischl B, FreeSurfer. NeuroImage. 2012;62:774–81. https://doi.org/10.1016/j.neuroimage.2012.01.021.
107. Frings L, Hellwig S, Spehl TS, Bormann T, Buchert R, Vach W, et al. Asymmetries of amyloid-β burden and neuronal dysfunction are positively correlated in Alzheimer's disease. Brain. 2015;138:3089–99. https://doi.org/10.1093/brain/awv229.
108. Shi F, Liu B, Zhou Y, Yu C, Jiang T. Hippocampal volume and asymmetry in mild cognitive impairment and Alzheimer's disease: Meta-analyses of MRI studies. Hippocampus. 2009;19:1055–64. https://doi.org/10.1002/hipo.20573.
109. Roe JM, Vidal-Piñeiro D, Sørensen Ø, Brandmaier AM, Düzel S, Gonzalez HA, et al. Asymmetric thinning of the cerebral cortex across the adult lifespan is accelerated in Alzheimer's disease. Nat Commun Nat Publishing Group. 2021;12:721. https://doi.org/10.1038/s41467-021-21057-y.
110. Kim JH, Lee JW, Kim GH, Roh JH, Kim M-J, Seo SW, et al. Cortical asymmetries in normal, mild cognitive impairment, and Alzheimer's disease. Neurobiol Aging. 2012;33:1959–66. https://doi.org/10.1016/j.neurobiolaging.2011.06.026.

111. Ozdemir RA, Passera B, Fried PJ, Press D, Shaughnessy LW, Buss S, et al. Neurophysiological signatures of default mode network dysfunction and cognitive decline in Alzheimer's disease. Sci Adv Am Association Advancement Sci. 2025;11:eadt8991. https://doi.org/10.1126/sciadv.adt8991.
112. Buckner RL, Snyder AZ, Shannon BJ, LaRossa G, Sachs R, Fotenos AF, et al. Molecular, structural, and functional characterization of Alzheimer's disease: Evidence for a relationship between default activity, amyloid, and memory. J Neurosci. 2005;25:7709–17. https://doi.org/10.1523/JNEUROSCI.2177-05.2005.
113. McDonald CR, Gharapetian L, McEvoy LK, Fennema-Notestine C, Hagler DJ, Holland D, et al. Relationship between regional atrophy rates and cognitive decline in mild cognitive impairment. Neurobiol Aging. 2012;33:242–53. https://doi.org/10.1016/j.neurobiolaging.2010.03.015.
114. Pini L, Wennberg AM, Salvalaggio A, Vallesi A, Pievani M, Corbetta M. Breakdown of specific functional brain networks in clinical variants of Alzheimer's disease. Ageing Res Reviews Elsevier. 2021;72:101482. https://doi.org/10.1016/J.ARR.2021.101482.
115. Sarazin M, Chauviré V, Gerardin E, Colliot O, Kinkingnéhun S, De Souza LC, et al. The Amnestic Syndrome of Hippocampal type in Alzheimer's Disease: An MRI Study. JAD. 2010;22:285–94. https://doi.org/10.3233/JAD-2010-091150.
116. Greicius MD, Supekar K, Menon V, Dougherty RF. Resting-State Functional Connectivity Reflects Structural Connectivity in the Default Mode Network. Cereb Cortex. 2009;19:72–8. https://doi.org/10.1093/cercor/bhn059.

Publisher's note Springer Nature remains neutral with regard to jurisdictional claims in published maps and institutional affiliations.

Authors and Affiliations

Giacomo Bertazzoli[1,2,3] · Elisa Canu[4,5] · Chiara Bagattini[6,7] · Fabiola Freri[4,5] · Natale Salvatore Bonfiglio[8] · Debora Brignani[1,9] · Martina Bulgari[1] · Veronica Castelnovo[4,5] · Mara Delai[1] · Elisabetta Ferrari[1] · Claudia Fracassi[1] · Peter J. Fried[2,3] · Delia Lucarelli[1,10,11] · Eleonora Marcantoni[1,12] · Moira Marizzoni[13] · Annamaria Cattaneo[13,14] · Valentina Nicolosi[15] · Giulia Quattrini[13,15] · Silvia Saglia[15,16] · Michela Pievani[15] · Vincenzo Romei[17] · Antonietta Stango[1] · Massimo Filippi[4,5,18,19,20] · Federica Agosta[4,5,18,20] · Marta Bortoletto[1,21]

✉ Giacomo Bertazzoli
gbertazz@bidmc.harvard.edu

✉ Marta Bortoletto
marta.bortoletto@imtlucca.it

1 Neurophysiology Lab, IRCCS Istituto Centro San Giovanni di Dio Fatebenefratelli, Via Pilastroni 4, Brescia, BS 25125, Italy

2 Department of Neurology, Berenson-Allen Center for Noninvasive Brain Stimulation, Beth Israel Deaconess Medical Center, 330 Brookline Avenue, Boston, MA 02215, USA

3 Department of Neurology, Harvard Medical School, 25 Shattuck Street, Boston, MA 02115, USA

4 Neuroimaging Research Unit, Division of Neuroscience, IRCCS San Raffaele Scientific Institute, Via Olgettina 60, Milan, MI 20132, Italy

5 Neurology Unit, IRCCS San Raffaele Scientific Institute, Via Olgettina 60, Milan, MI 20132, Italy

6 Section of Neurosurgery, Department of Neurosciences, Biomedicine and Movement Sciences, University of Verona, Ospedale Civile Maggiore di Borgo Trento, Piazzale Aristide Stefani 1, Verona, VR 37126, Italy

7 Perception and Awareness Lab, Department of Neurosciences, Biomedicine and Movement Sciences, University of Verona, Strada Le Grazie 8, Verona, VR 37134, Italy

8 Service of Statistics, IRCCS Istituto Centro San Giovanni di Dio Fatebenefratelli, Via Pilastroni 4, Brescia, BS 25125, Italy

[9] Department of Clinical and Experimental Sciences, Università degli Studi di Brescia, Viale Europa 11, Brescia, BS 25123, Italy

[10] Department of Neuroscience, Imaging and Clinical Sciences, G. d'Annunzio University of Chieti–Pescara, Via dei Vestini 31, Chieti, CH 66100, Italy

[11] Institute for Advanced Biomedical Technologies (ITAB), G. d'Annunzio University of Chieti–Pescara, Via Luigi Polacchi 11, Chieti, CH 66100, Italy

[12] Centre for Neurotechnology, School of Psychology and Neuroscience, University of Glasgow, 58 Hillhead Street, Glasgow G12 8QB, UK

[13] Biological Psychiatry Unit, IRCCS Istituto Centro San Giovanni di Dio Fatebenefratelli, Via Pilastroni 4, Brescia, BS 25125, Italy

[14] Department of Pharmacological and Biomolecular Sciences, University of Milan, Via Balzaretti 9, Milan, MI 20133, Italy

[15] Laboratory of Alzheimer's Neuroimaging and Epidemiology, IRCCS Istituto Centro San Giovanni di Dio Fatebenefratelli, Via Pilastroni 4, Brescia, BS 25125, Italy

[16] Department of Engineering for Innovation Medicine, University of Verona, Strada Le Grazie 15, Verona, VR 37134, Italy

[17] Centro Studi e Ricerche in Neuroscienze Cognitive, Dipartimento di Psicologia "Renzo Canestrari", Alma Mater Studiorum Università di Bologna, Campus di Cesena, Viale Rasi e Spinelli 176, Cesena, FC 47521, Italy

[18] Vita-Salute San Raffaele University, Via Olgettina 60, Milan, MI 20132, Italy

[19] Neurophysiology Service, IRCCS San Raffaele Scientific Institute, Via Olgettina 60, Milan, MI 20132, Italy

[20] Neurorehabilitation Unit, IRCCS San Raffaele Scientific Institute, Via Olgettina 60, Milan, MI 20132, Italy

[21] MoMiLab, IMT School for Advanced Studies, Piazza San Francesco 19, Lucca, LU 55100, Italy